[redacted]

57p

NASA TECHNICAL MEMORANDUM

NASA TM X-979

NASA TM X-979

X64 15867

Code 2 - Cat 04

CLASSIFICATION CHANGED
UNCLASSIFIED
TO
By Authority of TID 7/15 Date 12-27-71

LOW-SPEED AERODYNAMIC CHARACTERISTICS OF A SUPERSONIC TRANSPORT MODEL WITH A HIGH-ASPECT-RATIO VARIABLE-SWEEP WARPED WING

by Vernard E. Lockwood, Linwood W. McKinney, and John E. Lamar

Langley Research Center
Langley Station, Hampton, Va.

N71-70614
(ACCESSION NUMBER)
(THRU)
(CODE)
(CATEGORY)
57
(PAGES)
[redacted]
(NASA CR OR TMX OR AD NUMBER)
FACILITY FORM 602

NATIONAL AERONAUTICS AND SPACE ADMINISTRATION • WASHINGTON, D. C. • JULY 1964

[redacted]

[redacted]

LOW-SPEED AERODYNAMIC CHARACTERISTICS OF A SUPERSONIC TRANSPORT MODEL WITH A HIGH-ASPECT-RATIO VARIABLE-SWEEP WARPED WING

By Vernard E. Lockwood, Linwood W. McKinney, and John E. Lamar

Langley Research Center
Langley Station, Hampton, Va.

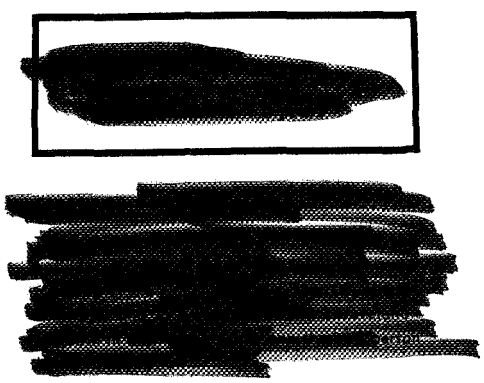

NATIONAL AERONAUTICS AND SPACE ADMINISTRATION

[redacted]

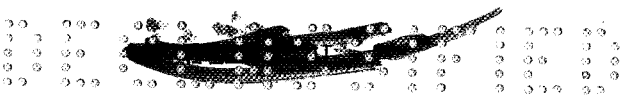

LOW-SPEED AERODYNAMIC CHARACTERISTICS OF A SUPERSONIC TRANSPORT MODEL WITH A HIGH-ASPECT-RATIO VARIABLE-SWEEP WARPED WING*

By Vernard E. Lockwood, Linwood W. McKinney, and John E. Lamar
Langley Research Center

SUMMARY

15867

A low-speed wind-tunnel investigation of the stability and control characteristics was made of a model of a proposed three-engine supersonic transport configuration. The model had a variable-sweep, cambered-and-twisted wing with an outboard-pivot location. Two engine nacelles were mounted below the wing on pylons supported from the fuselage, and a single-engine nacelle was mounted in the vertical tail just above the fuselage. Longitudinal stability and control characteristics were determined for a range of wing-sweep angles from 0° to 76°. Lateral stability characteristics were determined for wing sweeps of 16° and 76° and directional control characteristics were determined for a wing sweep of 16°. The investigation also included model breakdown tests to help determine factors affecting model stability. Additional tests were made with the horizontal tail in several vertical locations.

The results of the investigation show that the model, although longitudinally stable at low angles of attack, exhibited pitch-up in some part of the angle-of-attack range for all configurations and wing-sweep angles. The pitch-up, which began at an angle of attack as low as 5°, was caused by a combination of the nonlinear pitching moment of the wing-fuselage configuration reinforced by flow separation on the outer wing panel and the low horizontal-tail effectiveness. The aerodynamic-center variation between the design conditions of sweep (16° and 76°) was about 3.8 percent of model length.

The lift-drag ratios obtained for wing-sweep angles of 0°, 16°, and 31° were only slightly larger than the values obtained for a sweep angle of 46°; this result was attributed to the flow separation which occurred along the trailing edge of the wing and to the twist and camber designed into the wing for supersonic speeds. The directional stability of the model generally increased with angle of attack. Conf. Author

INTRODUCTION

For several years the National Aeronautics and Space Administration has been engaged in a research program to provide information relating to the design of a supersonic transport. Various design concepts involving the wing, fuselage, tail, and powerplant geometry have been explored. Several of these concepts have been tested over a wide Mach number range to determine their aerodynamic characteristics and to define problem areas. The results of some of the low-speed investigations of the conceptual designs are given in references 1 and 2 for fixed-wing configurations and in references 3 and 4 for variable-sweep configurations.

The present configuration, designated SCAT 16, had a variable-sweep wing and a three-engine propulsion arrangement. The wing panels in the design high-sweep condition were cambered and twisted for supersonic efficiency; in the low-sweep condition, this wing presented a high-aspect-ratio surface for efficient low-speed flight. Two engine nacelles were mounted below the wing on pylons supported from the fuselage, and one was mounted in the vertical tail just above the fuselage. The horizontal tail was attached in the wing-chord plane behind the wing.

The purpose of this investigation was to determine the low-speed aerodynamic characteristics of this high-aspect-ratio, variable-sweep, warped-wing configuration. Data were obtained to show the effect of wing sweep on longitudinal stability and control and on lateral and directional stability. Directional control characteristics were determined for a wing-sweep angle of 16°.

Because of longitudinal stability problems that became apparent during the investigation of the basic model, the scope of the investigation was enlarged. Model breakdown tests were made to aid in understanding the stability problems and a survey of horizontal-tail heights was made to determine the effect of horizontal-tail location.

The investigation was made in the Langley high-speed 7- by 10-foot tunnel at a dynamic pressure of 56.9 pounds per square foot, which corresponds to a Mach number of 0.2 and a Reynolds number of 1.41×10^{6} per foot. A smaller scale model was also tested at transonic and supersonic speeds; the results of this investigation are presented in reference 5.

SYMBOLS

Lift and drag coefficients are referred to stability axes, whereas the side-force, yawing-moment, pitching-moment, and rolling-moment coefficients are referred to the body-axis system, as shown in figure 1. The model moment reference is on the fuselage reference line at fuselage station 56.75. The reference dimensions used in reducing the data are given in the three-view drawing of figure 2 and table I. The reference area is the area bounded by the leading and trailing edges of the 16° swept wing which are extended to the plane of

symmetry. Table I also contains the dimensions of the 76° swept wing, which can can be used for converting the results contained herein to the reference basis used for reference 5.

C_D drag coefficient, $\frac{\text{Drag}}{qS}$

C_{D_o} estimated skin-friction drag coefficient

C_L lift coefficient, $\frac{\text{Lift}}{qS}$

C_l rolling-moment coefficient, $\frac{\text{Rolling moment}}{qSb}$

C_m pitching-moment coefficient, $\frac{\text{Pitching moment}}{qSc_{ref}}$

C_n yawing-moment coefficient, $\frac{\text{Yawing moment}}{qSb}$

C_Y side-force coefficient, $\frac{\text{Side force}}{qS}$

L/D lift-drag ratio, C_L/C_D

$(L/D)_{max}$ maximum lift-drag ratio

q dynamic pressure, lb/sq ft

S wing area, sq ft

b wing span, in.

c_{ref} reference chord, in.

α angle of attack of fuselage reference line, deg

β angle of sideslip, deg

$\Delta\beta$ increment of sideslip angle between $\beta = \pm 5^\circ$, corrected for balance and strut deflection, deg

Λ angle of wing leading-edge sweep, deg

Γ horizontal-tail dihedral (positive up), deg

δ_h horizontal-tail deflection (measured from wing reference plane), deg

δ_r rudder deflection, deg

$$C_{l_\beta} = \frac{\left(C_{l,\beta=5^\circ} - C_{l,\beta=-5^\circ}\right)}{\Delta\beta}$$

$$C_{n_\beta} = \frac{\left(C_{n,\beta=5^\circ} - C_{n,\beta=-5^\circ}\right)}{\Delta\beta}$$

$$C_{Y_\beta} = \frac{\left(C_{Y,\beta=5^\circ} - C_{Y,\beta=-5^\circ}\right)}{\Delta\beta}$$

$$\Delta C_{l_\beta} = \left(C_{l_\beta}\right)_{V\ on} - \left(C_{l_\beta}\right)_{V\ off}$$

$$\Delta C_{n_\beta} = \left(C_{n_\beta}\right)_{V\ on} - \left(C_{n_\beta}\right)_{V\ off} \quad \text{or} \quad \left(C_{n_\beta}\right)_{H\ on} - \left(C_{n_\beta}\right)_{H\ off}$$

$$\Delta C_{Y_\beta} = \left(C_{Y_\beta}\right)_{V\ on} - \left(C_{Y_\beta}\right)_{V\ off}$$

$$\Delta C_m = \left(C_m\right)_{H\ on;\delta_h=0^\circ} - \left(C_m\right)_{H\ off}$$

$\partial C_m / \partial C_L$ slope of pitching-moment-coefficient curve near $C_L = 0$

C_{L_α} slope of the lift-coefficient curve near $C_L = 0$, per deg

Configuration designations:

F fuselage with attached forewing

W movable wing panel

H horizontal tail (subscripts 1 to 5, fig. 5)

V vertical tail without engine nacelle

V_N vertical tail with engine nacelle

N fuselage-mounted engine nacelles

MODEL

A three-view drawing of the model is presented in figure 2. The model is a 1/24-scale version of a proposed supersonic commercial air transport designated SCAT 16. Although the model was tested through a wing-sweep range from 0° to 76°, the design minimum sweep of the configuration was 16°. The three nacelles were located as shown in figure 2: one mounted in the vertical tail and the other two mounted on pylons beneath the wing on either side of the fuselage.

The movable wing panel, which was twisted and cambered for supersonic efficiency, is shown in figure 3(a). The airfoil-section contours of the wing corresponding to the indicated fuselage stations with the wing in the design high-speed position are shown in figure 3(b). It will be noted that the wing thickness at the theoretical tip (fuselage station 93.824) is zero; this station was used in fairing the tip.

The fuselage cross-sectional contours at various fuselage stations for the model used in the investigation are shown in figure 4. The model fuselage contour remains broad in the vicinity of the empennage because of the use of a 2-inch-diameter sting to support the model.

The horizontal tail, which was tested at four heights and two dihedral angles, is shown in figures 2 and 5. The basic tail H_1 was located on the fuselage reference line and had 20° of negative dihedral; H_2 was the basic tail with no dihedral; and H_3, H_4, and H_5 were other vertical locations of the horizontal tail with no dihedral, as shown in figure 5.

The model had a 50-percent-chord rudder, as shown in figure 2.

TEST CONDITIONS AND CORRECTIONS

The investigation was made in the Langley high-speed 7- by 10-foot tunnel on a 1/24-scale model of SCAT 16. The model was sting mounted, as shown in figure 6. Forces and moments were measured by an internally mounted six-component strain-gage balance. To insure a turbulent boundary layer, transition strips of No. 100 carborundum grit approximately 1/8 inch wide were placed on the model at 7 percent of the length of the body and at 7 percent of the chord of the wing and all appendages.

The tests were made at a dynamic pressure of 56.9 pounds per square foot, which corresponds to a Mach number of 0.2 and a Reynolds number of 1.41×10^6 per foot. All configurations were tested through a range of angles of attack at 0° sideslip, and selected configurations were also tested at $\pm 5^\circ$ sideslip.

The drag data were corrected to correspond to a pressure at the base of the engine nacelles and the base of the fuselage equal to free-stream static pressure.

The nacelles had constant-diameter internal passages, for which an axial-force coefficient of 0.00254 for all three nacelles (0.00158 with lower nacelles and 0.00096 with upper nacelles) was calculated as being the internal skin friction due to flow through the nacelles. Where applicable, these values were subtracted from the drag coefficient in each test.

The jet-boundary corrections calculated for the drag and angle of attack by the method of reference 6 for the reference sweep condition are as follows:

$$C_D = (C_D)_{measured} + (0.006225)C_L^2$$

$$\alpha = \alpha_{measured} + (0.394000)C_L$$

The jet-boundary corrections to the pitching-moment data were found to be negligible.

The data were also corrected for wind-tunnel blockage by the method presented in reference 7.

The angles of attack and sideslip were corrected for deflection of the sting-support system under load.

PRESENTATION OF DATA

The results of the tests are presented in the following figures:

	Figure
Longitudinal characteristics:	
Effect of horizontal tail (H_1) at various wing-sweep angles	7-12
Effect of model components	13-15
Increment in pitching-moment coefficient due to addition of H_1 to various model component configurations	16
Effect of horizontal-tail vertical location	17
Increment in pitching-moment coefficient due to addition of H_1 to H_5 to complete model	18
Increment in pitching-moment coefficient due to wing sweep	19
Summary of longitudinal characteristics showing effect of sweep on C_{L_α}, $(L/D)_{max}$, and $\partial C_m/\partial C_L$	20
Lateral characteristics:	
Effect of nacelle configuration, $\Lambda = 16^\circ$ and $\Lambda = 76^\circ$	21
Effect of tail configuration, $\Lambda = 16^\circ$ and $\Lambda = 76^\circ$	22
Summary of tail effects on lateral characteristics	23
Effects of rudder deflection	24

Longitudinal Characteristics

Longitudinal stability and control characteristics of the SCAT 16 configuration were measured for a range of wing-sweep angles from 0° to 76°, with and without the basic horizontal-tail configuration. These data are presented in figures 7 to 12. The model, although longitudinally stable at low angles of attack within the design wing-sweep range ($\Lambda = 16^\circ$ to $\Lambda = 76^\circ$), exhibited pitch-up at the higher angles of attack for all wing-sweep angles investigated.

To assist in understanding the pitch-up problems of the configuration, the fuselage was tested alone and in combination with various other model components, and wing tuft studies were conducted. These data indicated that the pitch-up resulted from a basic nonlinear pitching-moment variation of the fuselage reinforced by flow separation of the movable wing panel.

Figure 13 presents data for the model breakdown configurations. The fuselage-alone data show an increasingly nonlinear variation of C_m with α for $\alpha > 8^\circ$. This variation is attributed to the nonlinear lift generated by the nose of the fuselage and the attached forewing which acts as a low-aspect-ratio lifting surface. This lift, through its long moment arm (about 60 percent of the fuselage length is ahead of the moment reference point), is reflected in the pitching-moment data.

Figure 13 also shows that the wing is a contributing factor in increasing the nonlinearity of C_m with α. Not only are the pitching moments more nonlinear for FWV than FV, but the pitch-up begins at a lower angle of attack. For example, with configuration FV the moment break starts at $\alpha = 8^\circ$, whereas with FWV the tendency to pitch-up starts at about 5°. Tuft studies made during the wind-tunnel investigation at $\Lambda = 16^\circ$ showed extensive flow separation in the vicinity of the wing trailing edge at $\alpha = 6^\circ$. It also showed that separation spread rapidly over the wing as the angle of attack was increased to 10°. The early separation probably results from the increased lift effectiveness of the forewing, which produces a strong vortex flow that induces high angularities on the outboard panels. However, it is probable that this separation and accompanying pitch-up tendency can be reduced somewhat by the use of flow-control devices similar to those used with the configuration shown in figure 11 of reference 8 (p. 251).

To determine factors affecting the tail contribution to longitudinal stability, the increments in pitching-moment coefficient ΔC_n due to the addition of the horizontal tail H_1 have been determined. These increments, which are presented in figure 16, show that the combination of nacelles and wing reduces the effectiveness of the horizontal tail, particularly at high angles of attack. This result indicates the desirability of moving the horizontal tail to a vertical location of lesser influence. As a result of these studies, tests were made with the horizontal tail moved to the locations shown in figure 5, and the results of these tests are presented in figure 17.

Of the various tail locations investigated the basic location with 20° negative dihedral (H_1) deferred pitch-up to the highest angle of attack, as shown in figure 17. Although the horizontal tails located on the vertical fin (configurations H_3 and H_4), produced increased stability at low angles of attack, they also contributed to the model pitch-up. The increment in pitching-moment coefficient due to the horizontal tail at various locations is shown in figure 18. All configurations show losses in tail effectiveness at high angles of attack; this is an area in which increased effectiveness is needed to counter the pitch-up tendencies of the wing-fuselage combination. The basic tail H_1 is the best in this respect in that effectiveneness was maintained to a higher angle of attack than with any other horizontal tail investigated. The H_5 tail underneath the fuselage (which is only of academic interest since it is directly behind the engines) was less effective at low angles of attack than any of the other tail configurations; however, at $\alpha \approx 10^\circ$, increased effectiveness was noted for this configuration. The low effectiveness of the H_5 tail is probably due to wake effects of the nacelles and the fact that its effective span is greatly reduced by the presence of the fuselage. It is noted that the model was built to take a 2-inch-diameter sting at the base of the fuselage with normal clearances around it; hence, the fuselage was wider than for an actual airplane, so that the data for all tail positions may be affected to some degree by its width.

The wing-sweep effect on pitch-up is very pronounced, as indicated by a comparison of the pitching-moment-coefficient curves of figures 7 to 12. The variation is one from pitch-down for $\Lambda = 0^\circ$ (fig. 7) to one of extreme pitch-up for $\Lambda = 46^\circ$ (fig. 10). However, as wing sweep is increased to 61° and 76° (figs. 11 and 12), a pitch-down is encountered at the higher angles of attack.

At the higher wing sweeps, the wing separation and the fuselage effects produce additive moments resulting in extreme variations in aerodynamic center with angle of attack. For the wing with the 46° sweep angle, this shift amounts to about one reference chord or about 10.9 percent of the model length. The effects of wing sweep on the increment in pitching-moment coefficients due to the addition of the basic horizontal tail H_1 are shown in figure 19. In general, wing sweep has little effect on tail effectiveness up to an angle of attack of about 12°. At $\alpha \approx 12^\circ$ the tail effectiveness appears to be a function of the wing-sweep angle. The effectiveness is generally maintained to higher angles of attack as the sweep angle is increased from 0° to 76°.

Aerodynamic-center variations with sweep for the model with and without the horizontal tail are shown in figure 20. The SCAT 16 configuration shows the usual variation in aerodynamic center with wing sweep obtained with configurations of its type; first, a rearward shift is noted as the sweep is increased, followed by a forward shift at high sweep angles. The overall variation of $\partial C_m/\partial C_L$ with Λ is about 57 percent of the reference chord, and the change between 16° and 76° is about 36 percent of the reference chord. The change in $\partial C_m/\partial C_L$ between $\Lambda = 16^\circ$ and $\Lambda = 76^\circ$ represents about 3.8 percent of the model length and is large by any standard.

The maximum lift-drag ratios obtained for the models with low sweep angles (0° to 31°) appear to be low, since these ratios are only slightly in excess of the values for the model with $\Lambda = 46^\circ$, as is shown in figure 20. As a guide to what might be expected, values based on the equation

$$(L/D)_{max} = \sqrt{\frac{0.90\pi b^2}{4SC_{D_o}}}$$

are included in figure 20, where C_{D_o} equals the turbulent-skin-friction drag coefficient at model scale and 0.90 is the span efficiency factor. The calculated values show that much larger values of $(L/D)_{max}$ should have been realized for wing sweeps from 0° to 31°. It is believed that the major difference is due to the separation that occurred on the wing trailing edge at angles of attack in the vicinity of $(L/D)_{max}$. Some decrease in $(L/D)_{max}$ may be due to the twist-and-camber distribution designed into the wing for supersonic considerations.

Lateral Characteristics

The model exhibited positive directional stability throughout the test angle-of-attack range, as measured by C_{n_β} (fig. 21). The directional stability increased with angle of attack to a greater degree than normally expected. (For example, see ref. 4.) This increase of C_{n_β}, together with the positive trends of C_{Y_β} with α, indicates that a force opposed to the normal cross-flow component was probably developed on the long nose of the model. Previous experience with two-dimensional noncircular cross sections (ref. 9) has shown that cross-wind forces that are opposite to those generally expected can develop on cylinders at a certain Reynolds number and model orientation. The data of figure 14(a) in reference 9, which are for a cross section somewhat similar to the present model, give the two-dimensional results and their application to three-dimensional bodies at combined angles of attack and sideslip.

The effect of engine nacelles on the directional stability of the model is relatively small, as shown in figure 21. The most noticeable effect occurred for a wing sweep of 16°, at which the presence of the nacelles, V_N and N, resulted in reductions of C_{n_β} from $\alpha = 12^\circ$ to $\alpha = 23^\circ$.

A comparison of figure 22(a) with figure 22(b) shows that wing-sweep position is an important factor in the directional stability of the model at high angles of attack. Of the two sweep angles investigated, the 76° wing-sweep position contributed much greater stability; for example, at $\alpha = 18^\circ$, model FWH_1V_NN with $\Lambda = 76^\circ$ had a value of C_{n_β} of 0.007, whereas the model with $\Lambda = 16^\circ$ had a value of C_{n_β} of 0.004. This difference in stability can be traced, in part, to the difference in contributions of the vertical and

horizontal tails, as shown in figure 23. The contribution of the horizontal tail at 20° negative dihedral generally decreases as the angle of attack increases and becomes negative for $\Lambda = 16^\circ$ at $\alpha > 11^\circ$. The vertical-tail contribution to stability also shows a decrease at $\alpha > 12^\circ$ for $\Lambda = 16^\circ$. These losses in tail effectiveness plus the losses noted for the engine nacelle approximately account for the noticeable difference in ΔC_{n_β} between $\Lambda = 16^\circ$ and $\Lambda = 76^\circ$.

The effective dihedral parameter $-C_{l_\beta}$ given in figures 21 and 22 varies in a manner similar to that for other variable-sweep configurations of this type. That is, the models with the low-wing-sweep angle ($\Lambda = 16^\circ$) give increasing values of $-C_{l_\beta}$ up to wing-stall angle and then give decreasing values of $-C_{l_\beta}$ as the angle of attack is further increased. In contrast to this, the models with the high-sweep angle ($\Lambda = 76^\circ$) show increasing values of $-C_{l_\beta}$, as is typical of highly swept wings.

The effects of rudder deflection on the control characteristics of the complete model are shown in figure 24. The effectiveness is fairly constant over the angle-of-attack range investigated but, due to its short span, its effectiveness is limited; 24° of rudder deflection will trim out only 6.5° of sideslip, wings level.

CONCLUSIONS

Results of a preliminary low-speed stability and control investigation of a 1/24-scale model of a proposed supersonic transport configuration are summarized as follows:

1. The model, which was longitudinally stable at low angles of attack, exhibited pitch-up in the higher part of the test angle-of-attack range for all configurations and wing-sweep angles of 16° to 76°. The pitch-up, which began at an angle of attack as low as 5°, was caused by a combination of the nonlinear pitching moment of the wing-fuselage configuration reinforced by flow separation on the outer wing panel and the low horizontal-tail effectiveness.

2. The aerodynamic-center variation between the design conditions of 16° to 76° wing-sweep angles was about 36 percent of the reference chord (approximately 3.8 percent of the model length).

3. The lift-drag ratios obtained for 0°, 16°, and 31° wing sweeps were only slightly larger than the values obtained for 46° sweep; this was attributed to the flow separation that occurred along the trailing edge of the wing and to the twist and camber designed into the wing for supersonic speeds.

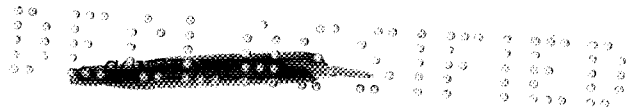

4. The directional stability of the model generally increased with angle of attack. This increase was attributed, in part, to the generation of a favorable side force on the long noncircular nose of the basic model.

5. The effective dihedral varied in a manner typical of that experienced by other variable-sweep configurations; that is, it increased through the angle-of-attack range for models with 76° of wing sweep and it decreased after wing stall for models with 16° of wing sweep.

6. The 50-percent-chord semispan rudder deflected 24° was effective in trimming out about 6.5° sideslip.

Langley Research Center,
National Aeronautics and Space Administration,
Langley Station, Hampton, Va., April 2, 1964.

REFERENCES

1. Koenig, David G., Brady, James A., and Page, V. Robert: Large-Scale Wind-Tunnel Tests at Low Speed of a Delta Winged Supersonic Transport Model in the Presence of the Ground. NASA TM X-644, 1962.

2. Whitcomb, Richard T., Patterson, James C., Jr., and Kelly, Thomas C.: An Investigation of the Subsonic, Transonic, and Supersonic Aerodynamic Characteristics of a Proposed Arrow-Wing Transport Airplane Configuration. NASA TM X-800, 1963.

3. Alford, William J., Jr., Hammond, Alexander D., and Henderson, William P.: Low-Speed Stability Characteristics of a Supersonic Transport Model With a Blended Wing-Body, Variable-Sweep Auxiliary Wing Panels, Outboard Tail Surfaces, and Simplified High-Lift Devices. NASA TM X-802, 1963.

4. Ward, Robert J., and McKee, John W.: Low-Speed Aerodynamic Stability and Control Characteristics of a Cambered Fuselage, Variable-Sweep Supersonic Transport Configuration. NASA TM X-632, 1962.

5. Fuller, Dennis E., and Weirich, Robert L.: Aerodynamic Characteristics at Mach Numbers From 0.50 to 2.96 of a Supersonic Transport Model With a Variable-Sweep High-Panel-Aspect-Ratio Wing. NASA TM X-980, 1964.

6. Gillis, Clarence L., Polhamus, Edward C., and Gray, Joseph L., Jr.: Charts for Determining Jet-Boundary Corrections for Complete Models in 7- by 10-Foot Closed Rectangular Wind Tunnels. NACA WR L-123, 1945. (Formerly NACA ARR L5G31.)

7. Herriot, John G.: Blockage Corrections for Three-Dimensional-Flow Closed-Throat Wind Tunnels, With Consideration of the Effect of Compressibility. NACA Rep. 995, 1950. (Supersedes NACA RM A7B28.)

8. Alford, William J., Jr., Lockwood, Vernard E., McKinney, Linwood W., and Greif, Richard K.: Stability and High-Lift Studies Applicable to Variable-Sweep Supersonic-Transport Configurations. Proceedings of NASA Conference on Supersonic-Transport Feasibility Studies and Supporting Research - September 17-19, 1963. NASA TM X-905, 1963, pp. 223-255.

9. Polhamus, Edward C., Geller, Edward W., and Grunwald, Kalman J.: Pressure and Force Characteristics of Noncircular Cylinders as Affected by Reynolds Number With a Method Included for Determining the Potential Flow About Arbitrary Shapes. NASA TR R-46, 1959.

TABLE I.- MODEL DIMENSIONS

Fuselage:	
Length, in.	91.00
Base area, sq ft	0.080
Chamber area, sq ft	0.034
Wing:	
Leading-edge sweep, reference, deg	16.0
Trailing-edge sweep, deg	7.3
Root chord, reference, in.	9.93
Tip chord, in.	3.29
Span, reference, in.	85.84
Area, reference, sq ft	3.94
Aspect ratio	12.99
Taper ratio	0.331
Horizontal tail H_1:	
Leading-edge sweep angle, deg	65.4
Trailing-edge sweep angle, deg	47.0
Root chord, in.	13.56
Tip chord, in.	3.86
Span, total, in.	18.96
Exposed area, sq ft	0.889
Dihedral angle, deg	-20.0
Vertical tail:	
Leading-edge sweep angle, deg	37.3
Trailing-edge sweep angle, deg	13.2
Root chord, in.	14.00
Tip chord, in.	2.80
Span, exposed, in.	10.38
Area, exposed, sq ft	0.606
Aspect ratio, exposed	1.24
Wing (included for comparison with ref. 5):	
Leading-edge sweep, deg	76.0
Span, in.	36.98
Area (leading and trailing edges extended to plane of symmetry), sq ft	5.729
Mean geometric chord, in.	30.78

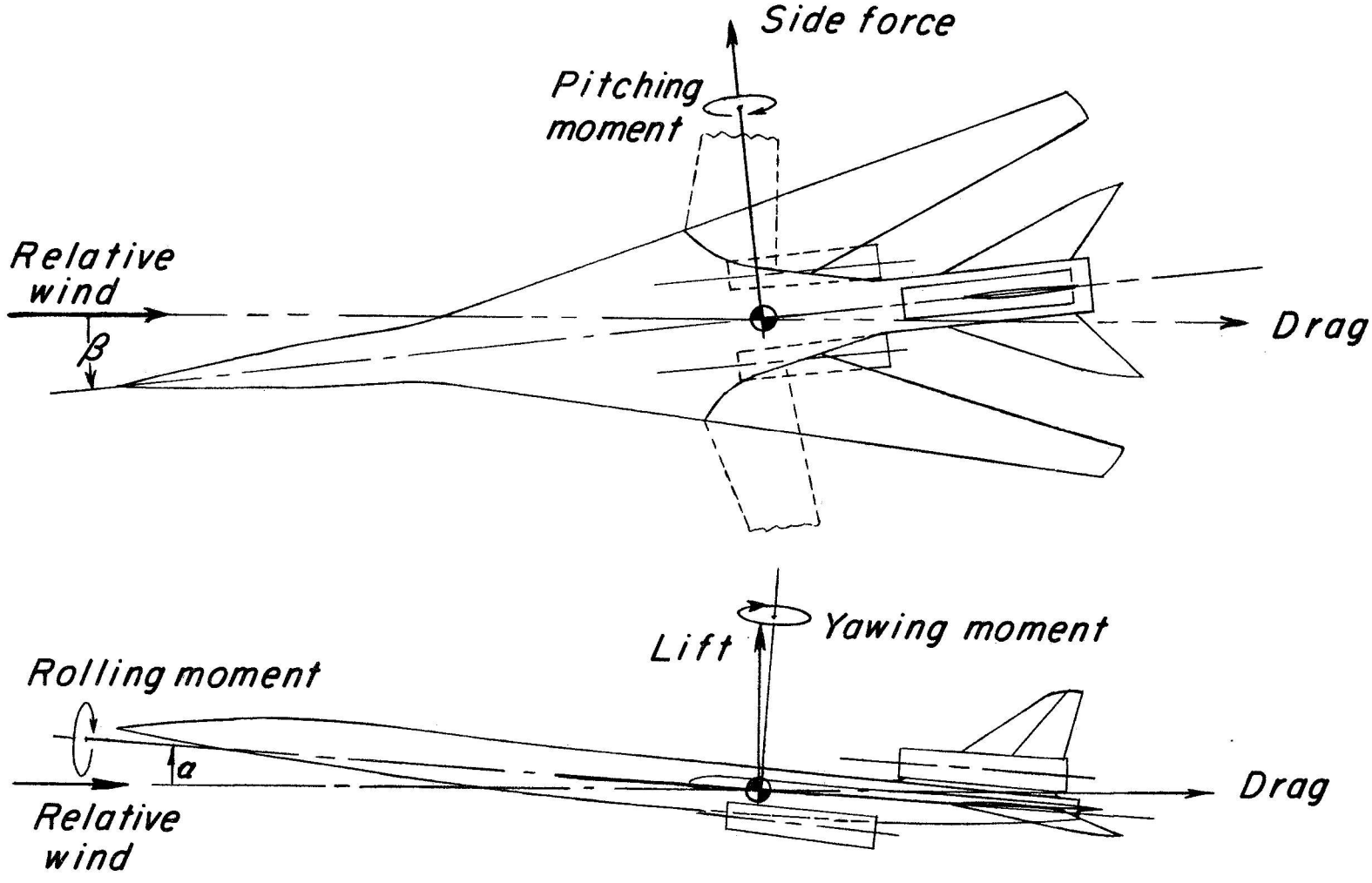

Figure 1.- System of axes used in presentation of data.

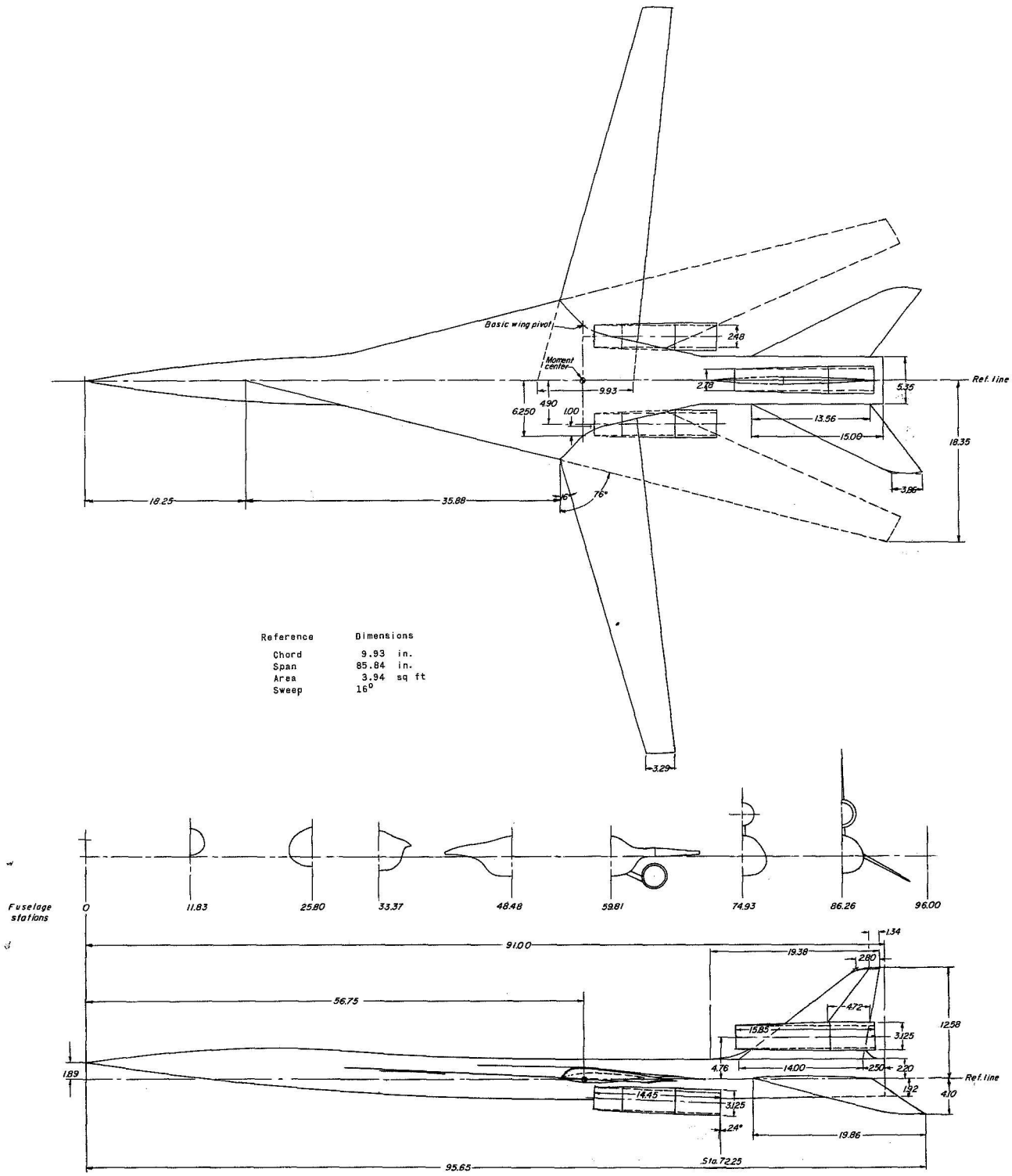

Figure 2.- Three-view drawing of model. All linear dimensions are in inches.

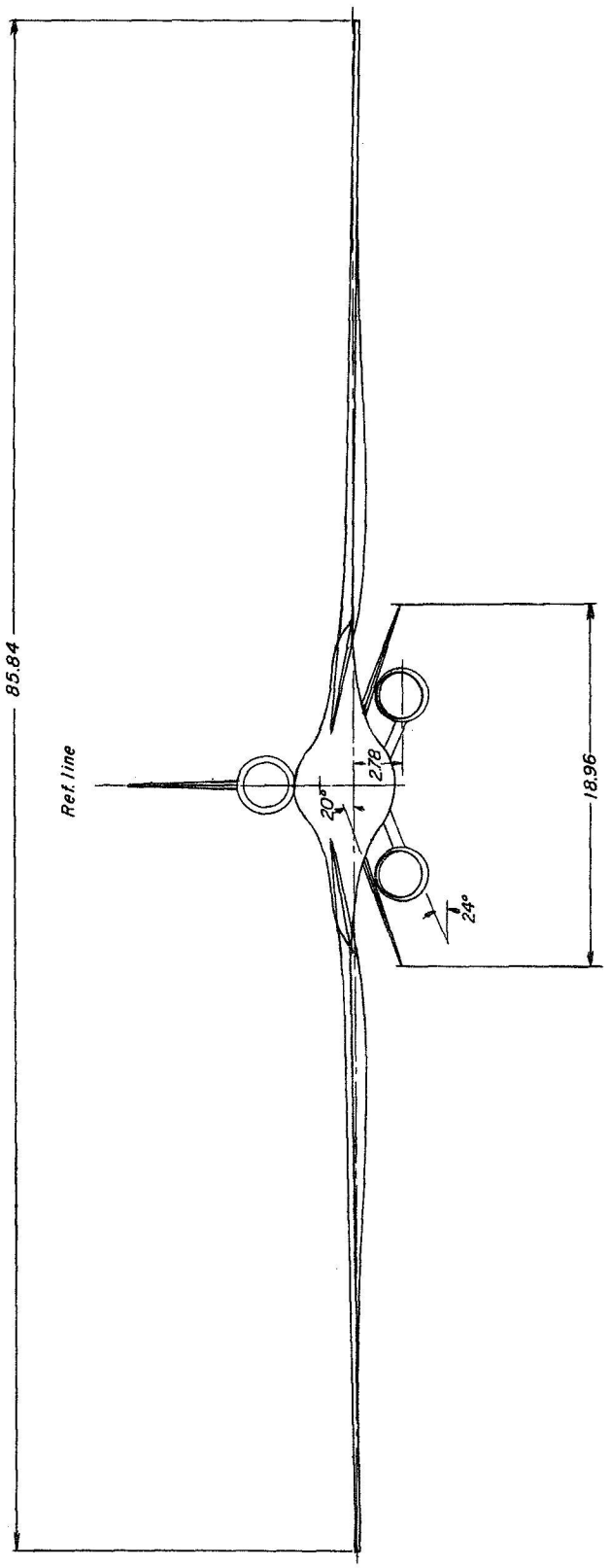

Figure 2.- Concluded.

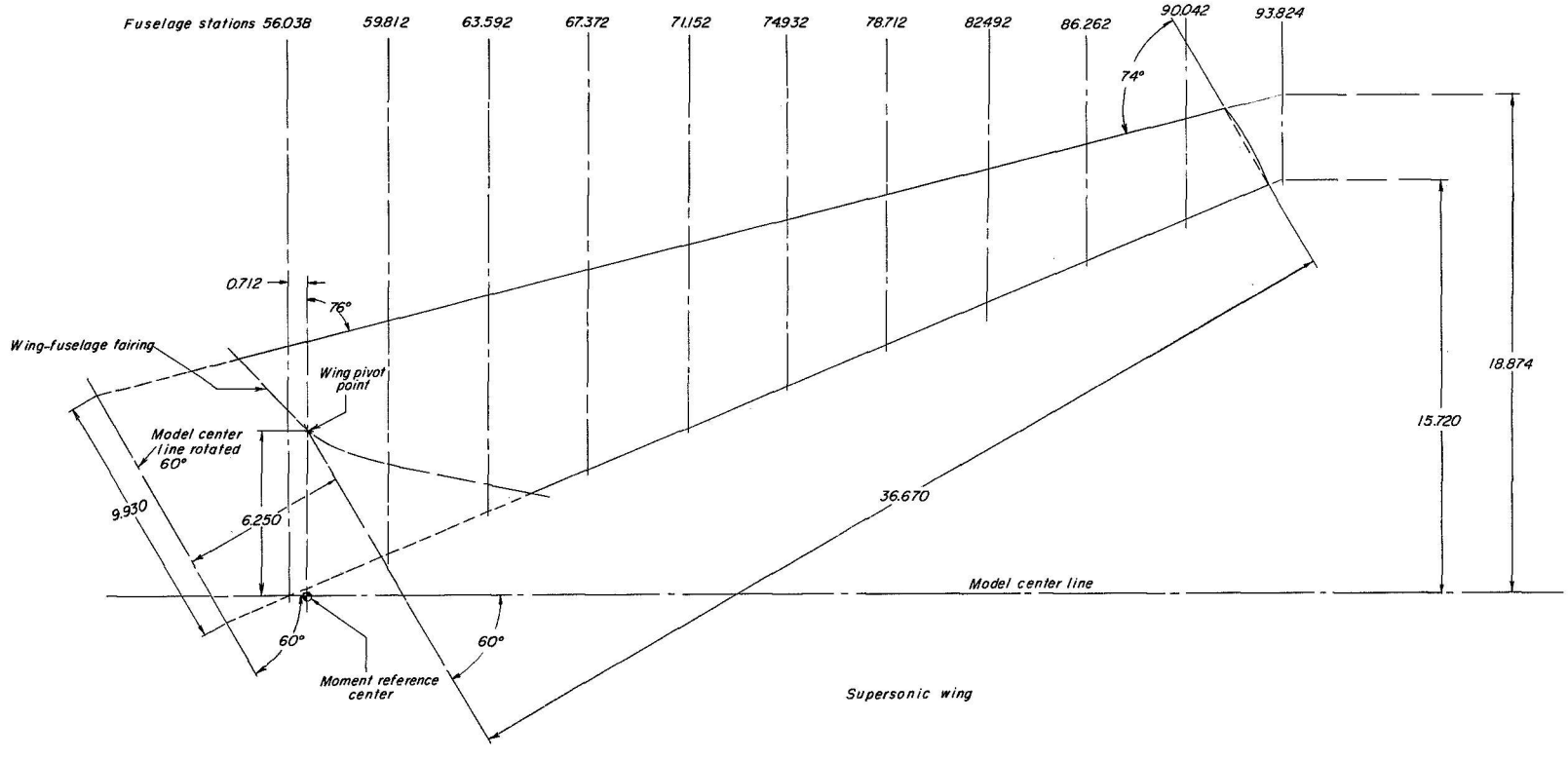

(a) Planform.

Figure 3.- Drawing of wing.

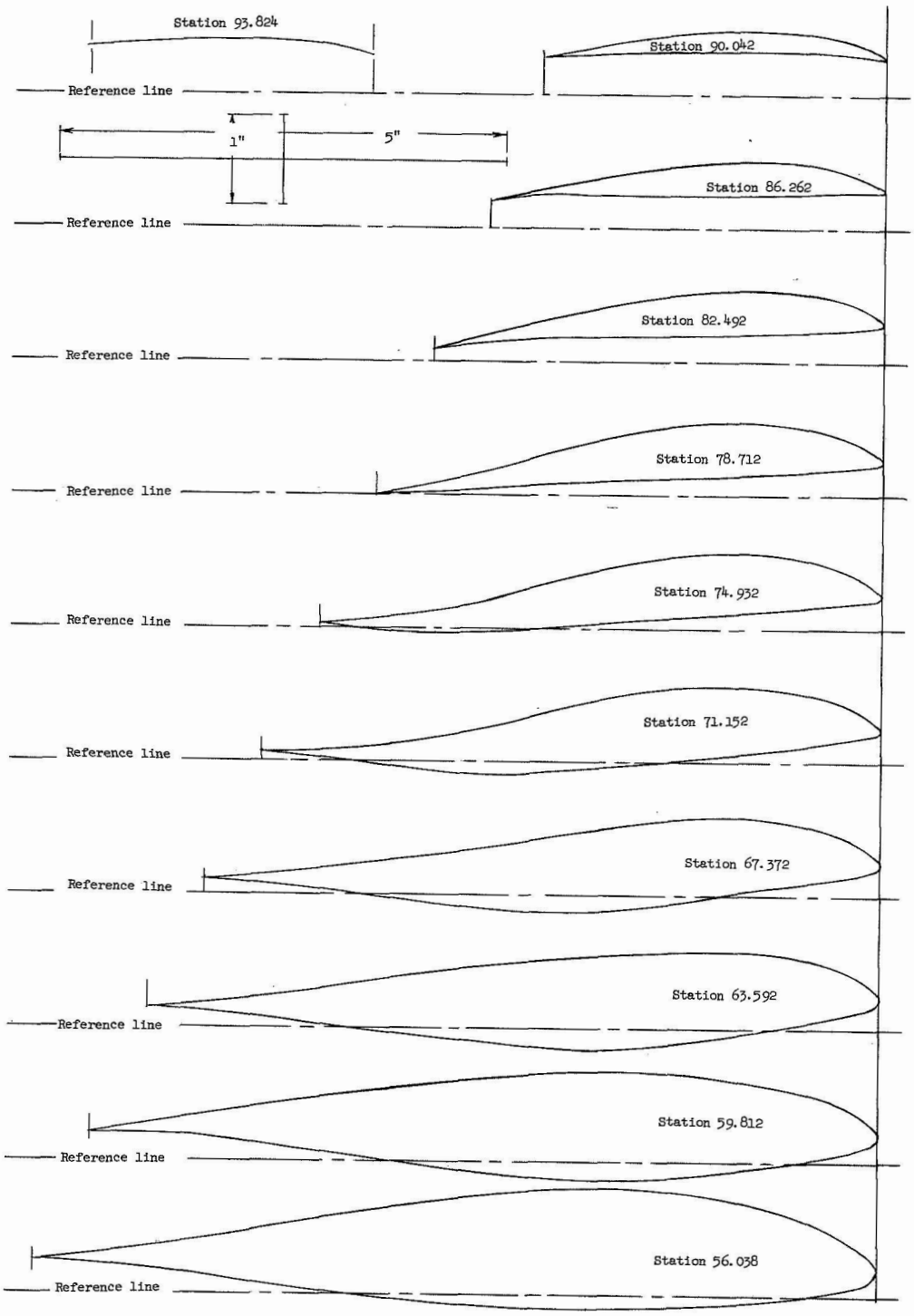

(b) Airfoil sections.

Figure 3.- Concluded.

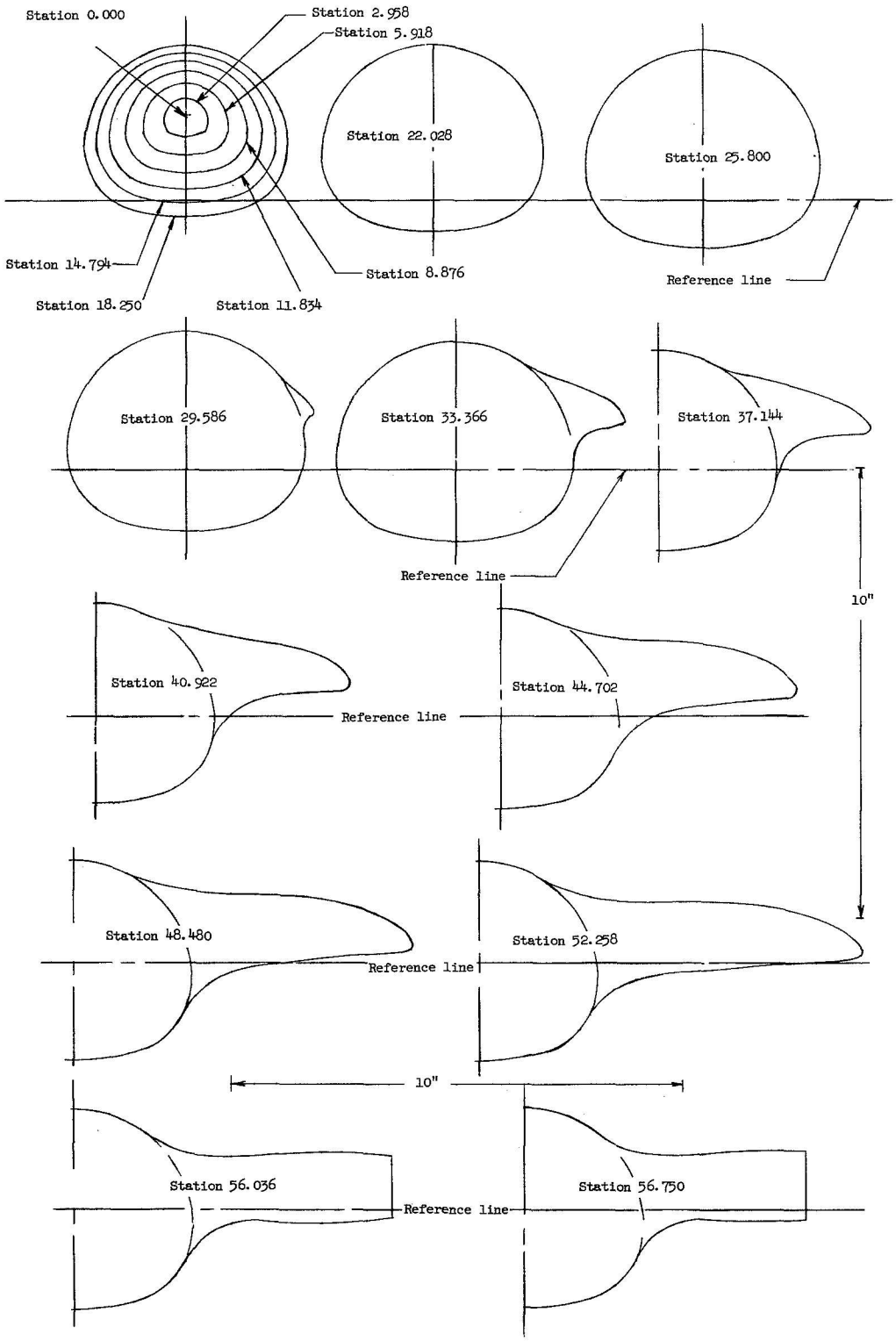

Figure 4.- Fuselage cross sections.

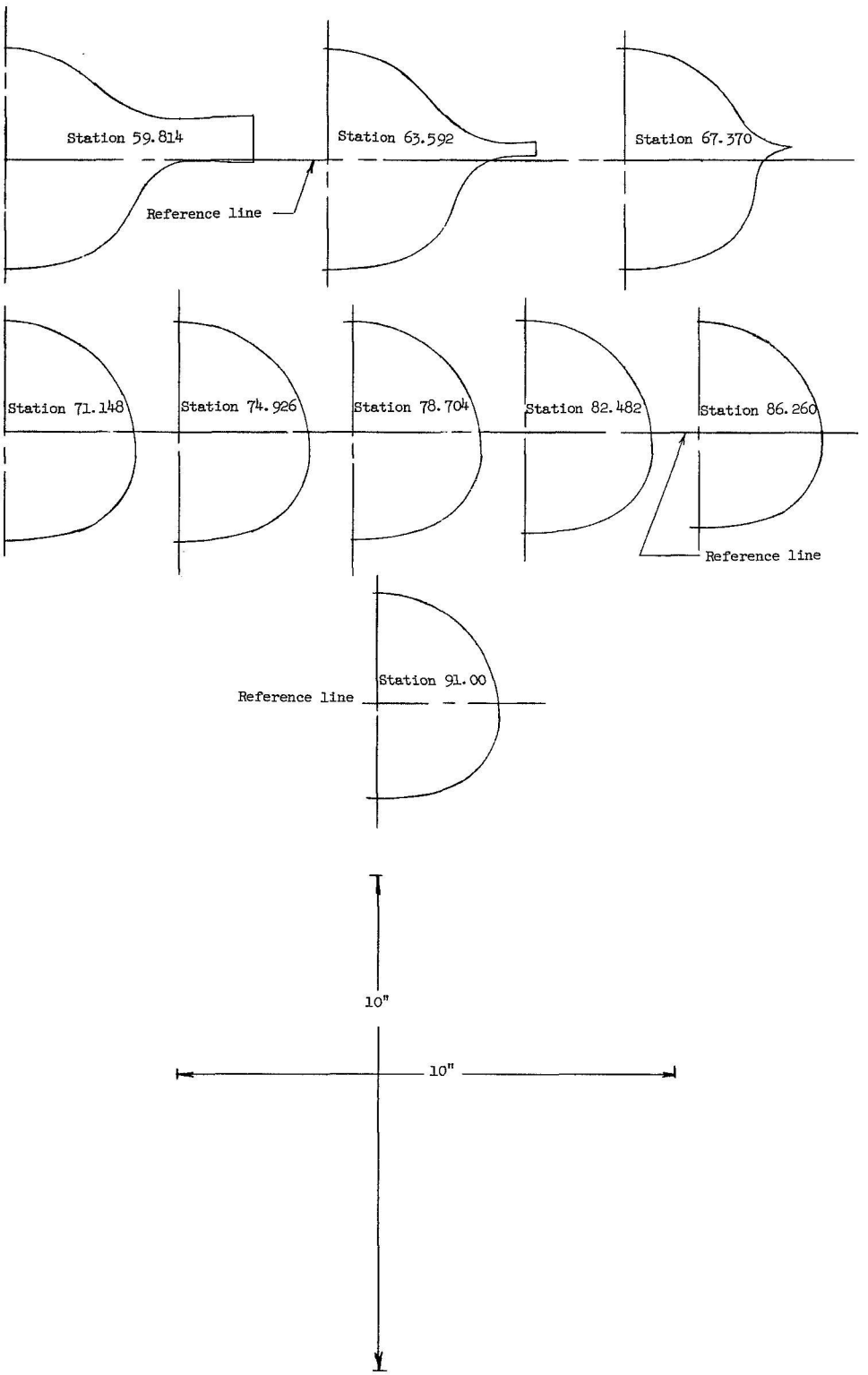

Figure 4.- Concluded.

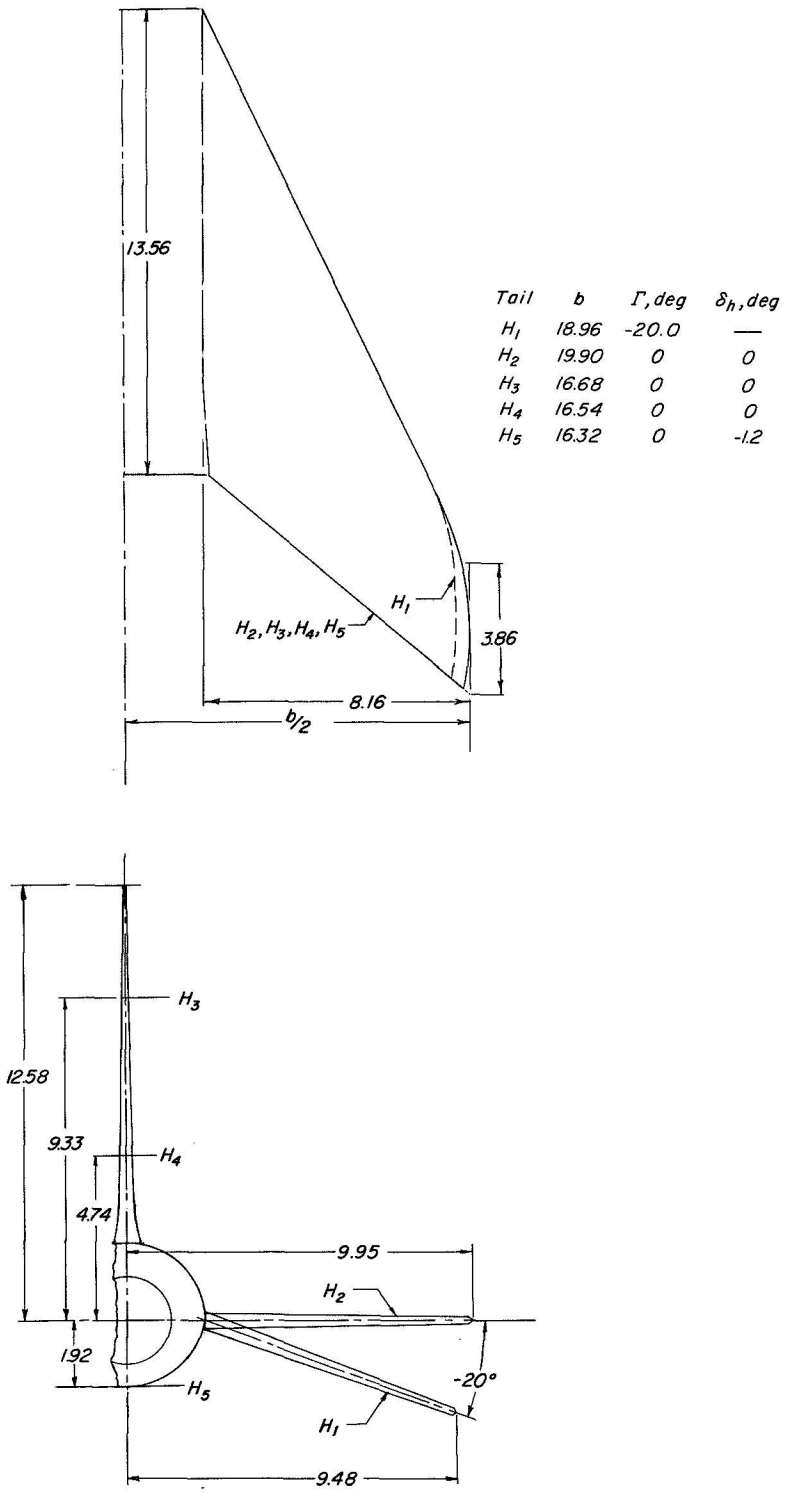

Tail	b	Γ, deg	δ_h, deg
H_1	18.96	-20.0	—
H_2	19.90	0	0
H_3	16.68	0	0
H_4	16.54	0	0
H_5	16.32	0	-1.2

Figure 5.- Horizontal-tail configurations. All dimensions are in inches unless otherwise noted.

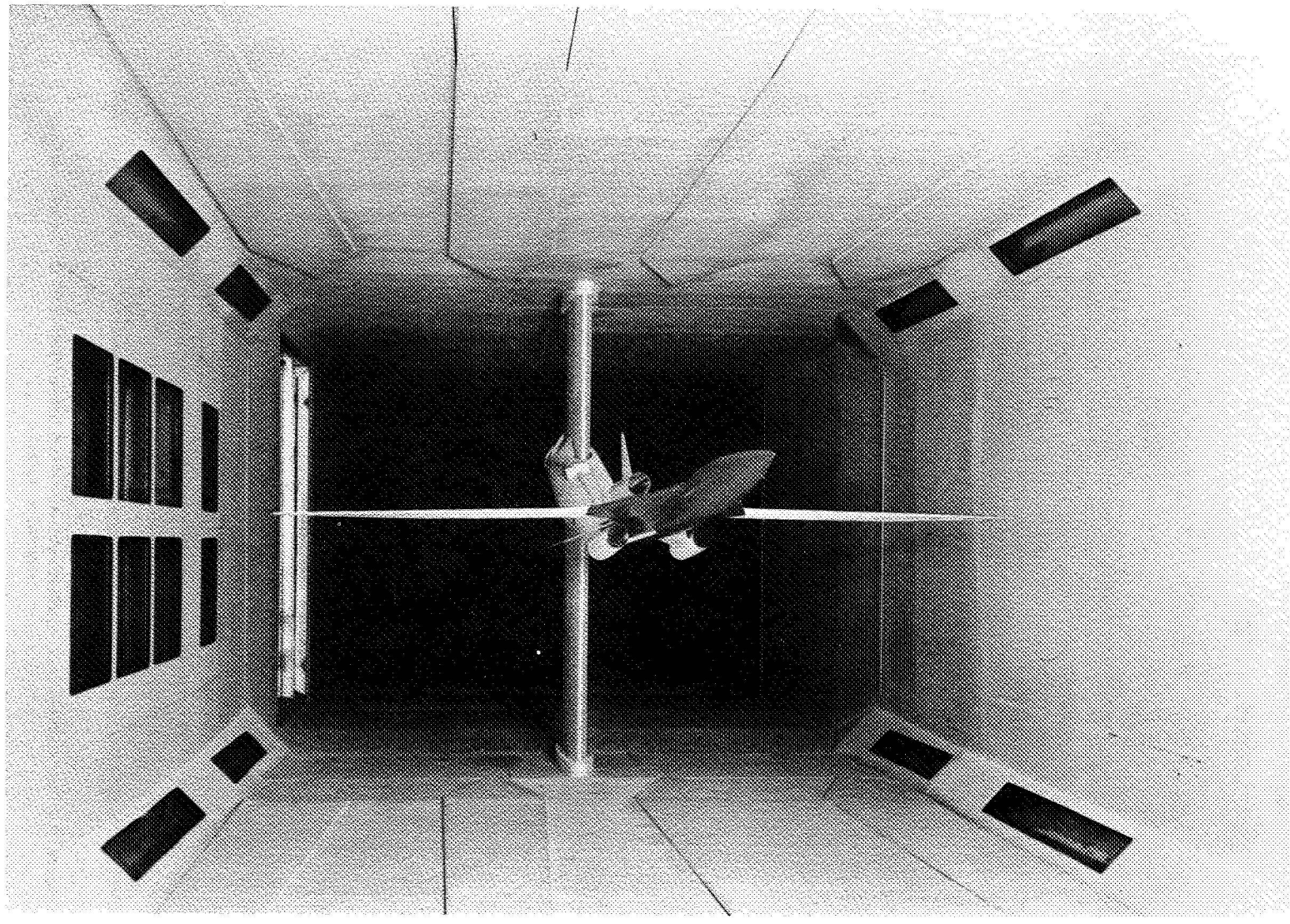

(a) $\Lambda = 16^{\circ}$.

L-62-8932

Figure 6.- Photograph of model in Langley high-speed 7- by 10-foot tunnel.

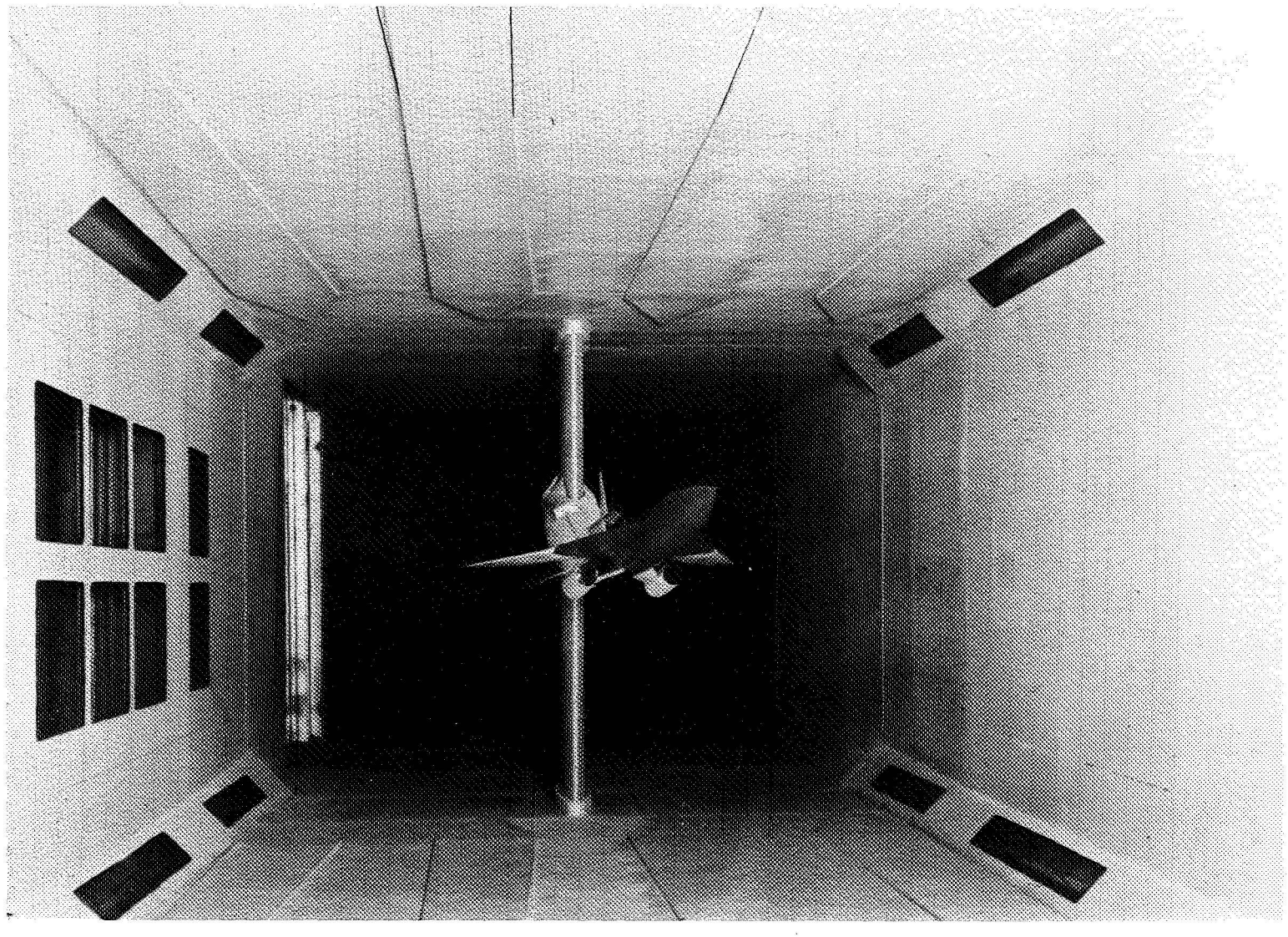

(b) $\Lambda = 76^{\circ}$.

L-62-8931

Figure 6.- Concluded.

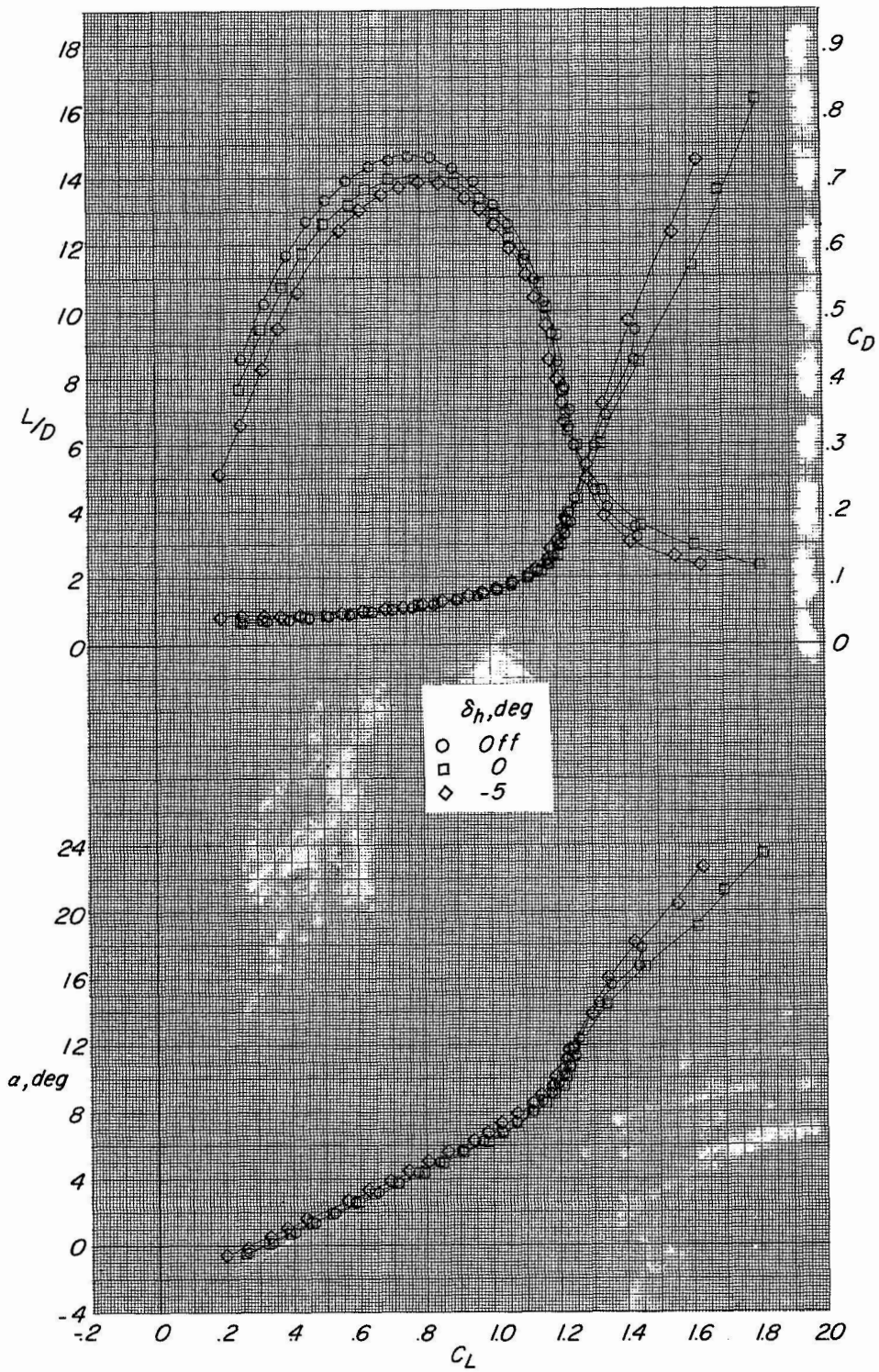

Figure 7.- Effect of horizontal tail on longitudinal aerodynamic characteristics. FWH_1V_TN; $\Lambda = 0^\circ$.

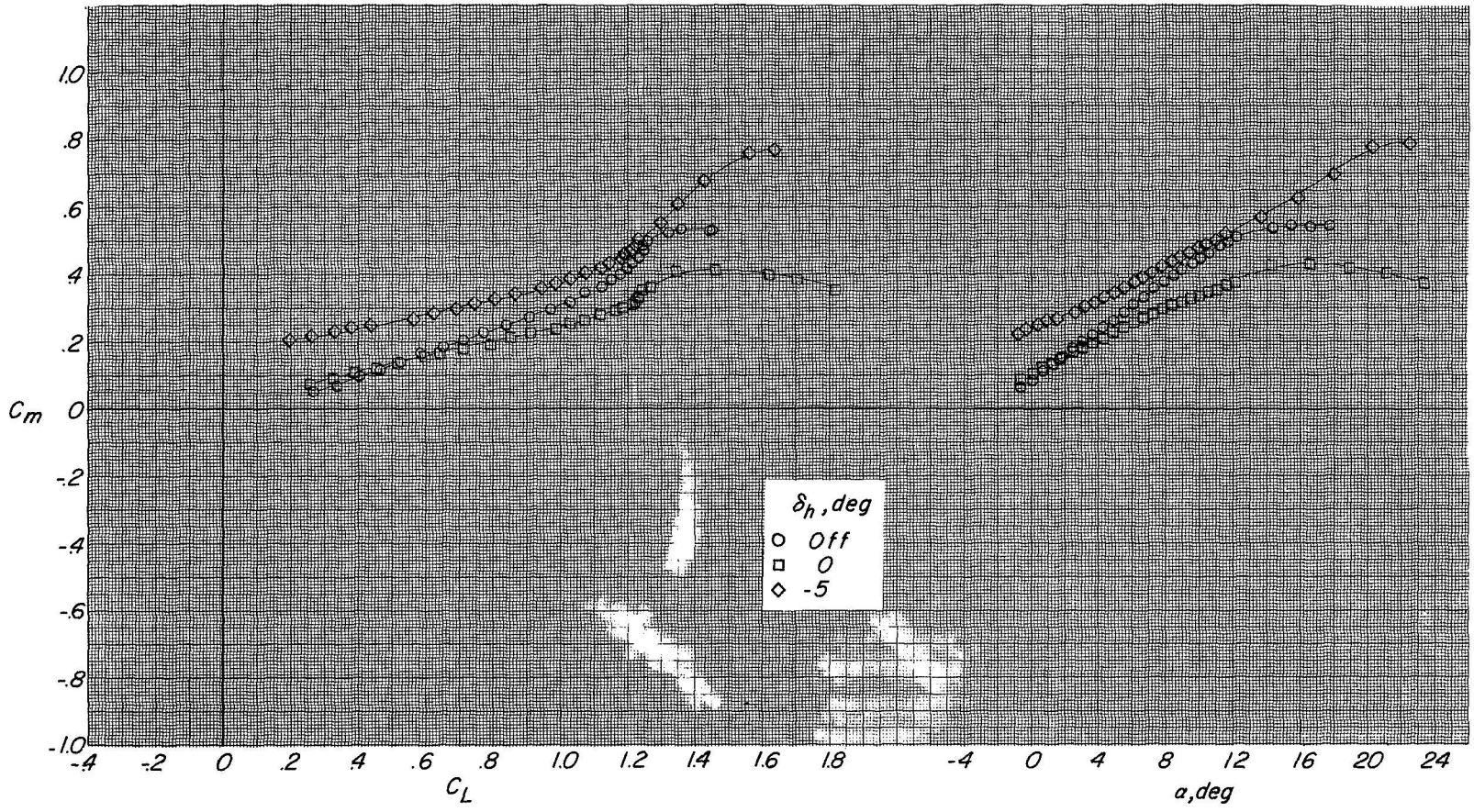

Figure 7.- Concluded.

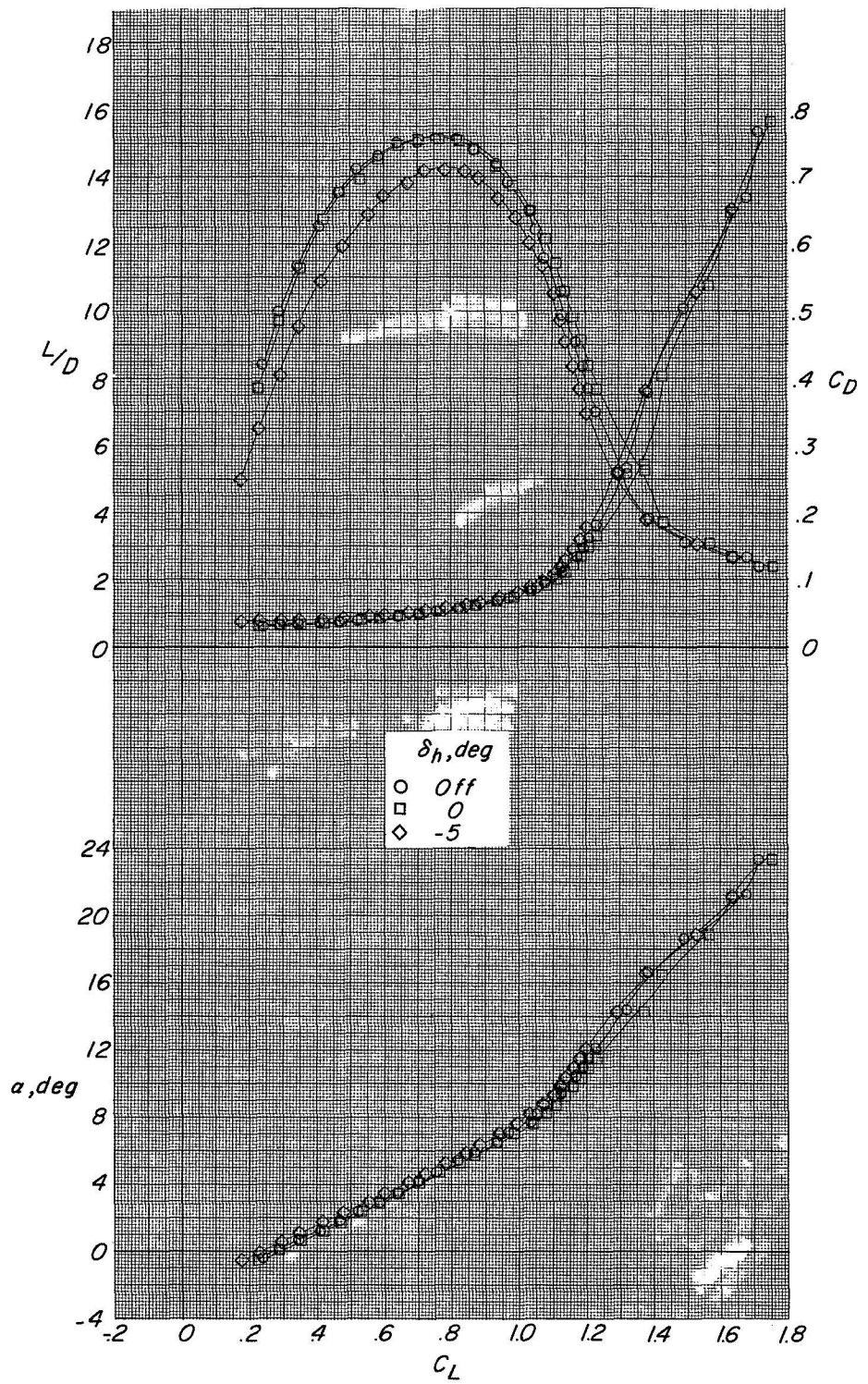

Figure 8.- Effect of horizontal tail on longitudinal aerodynamic characteristics. FWH_1V_TN; $\Lambda = 16^\circ$.

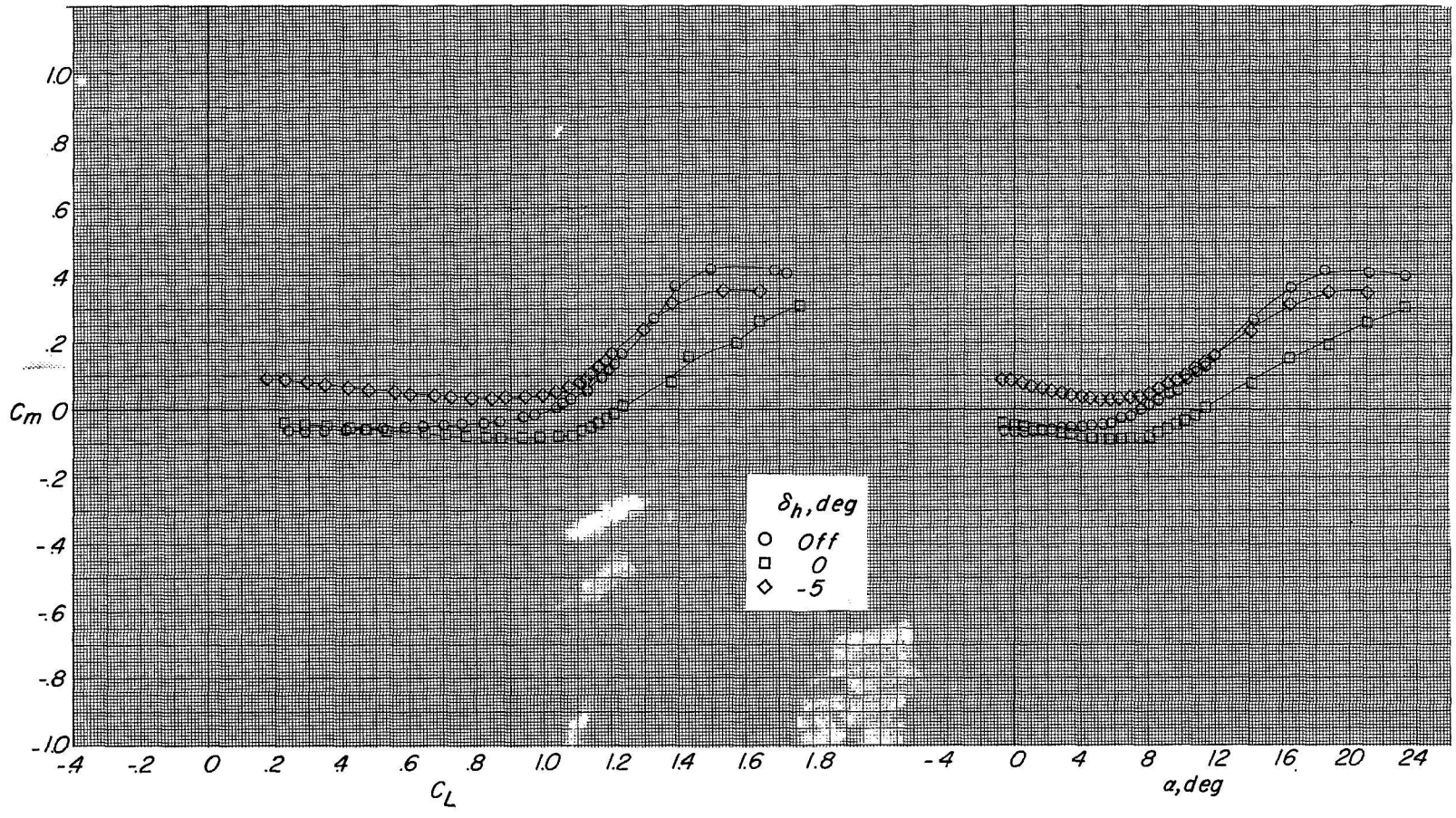

Figure 8.- Concluded.

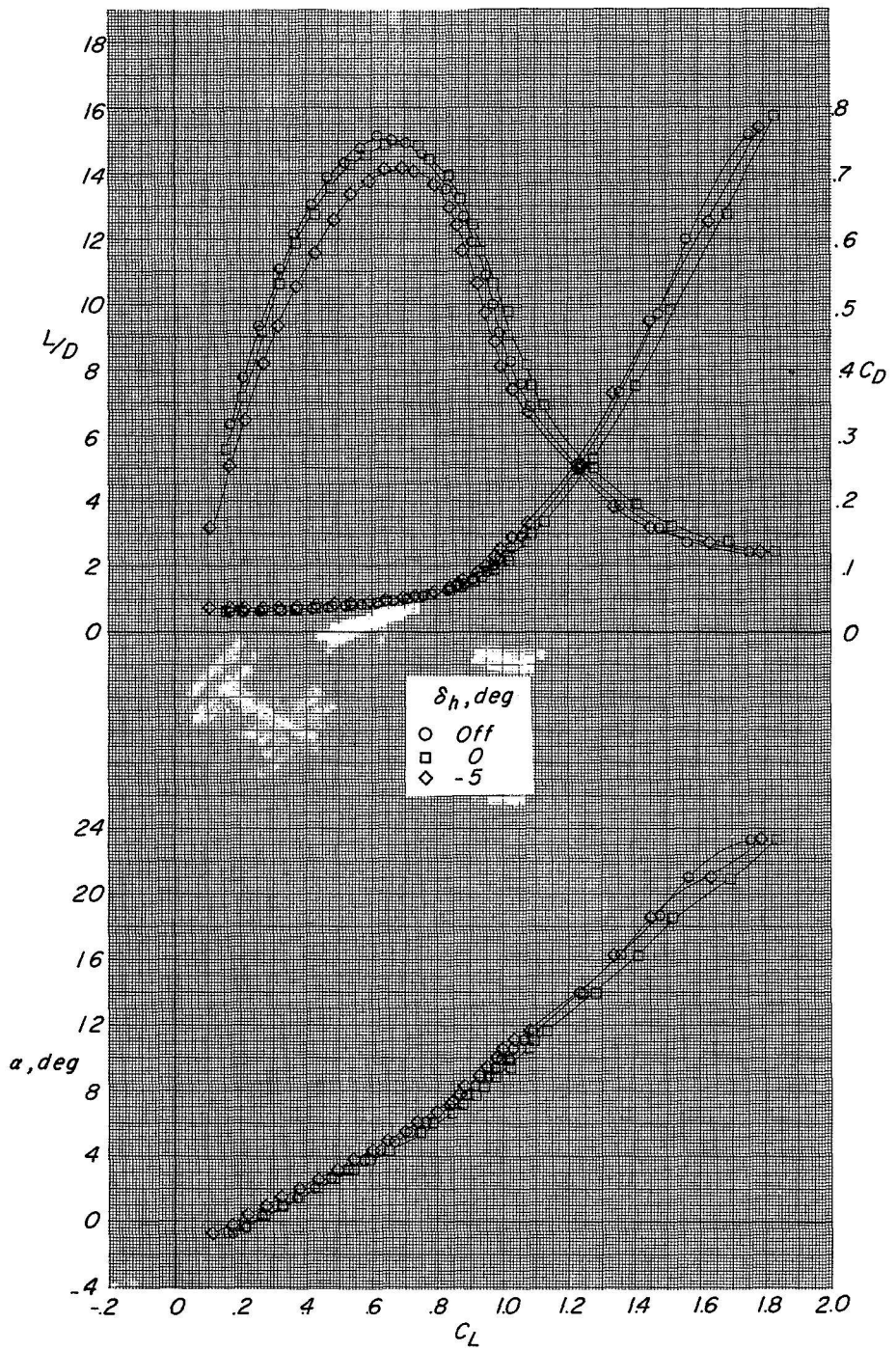

Figure 9.- Effect of horizontal tail on longitudinal aerodynamic characteristics. FWH_1V_NN; $\Lambda = 31^\circ$.

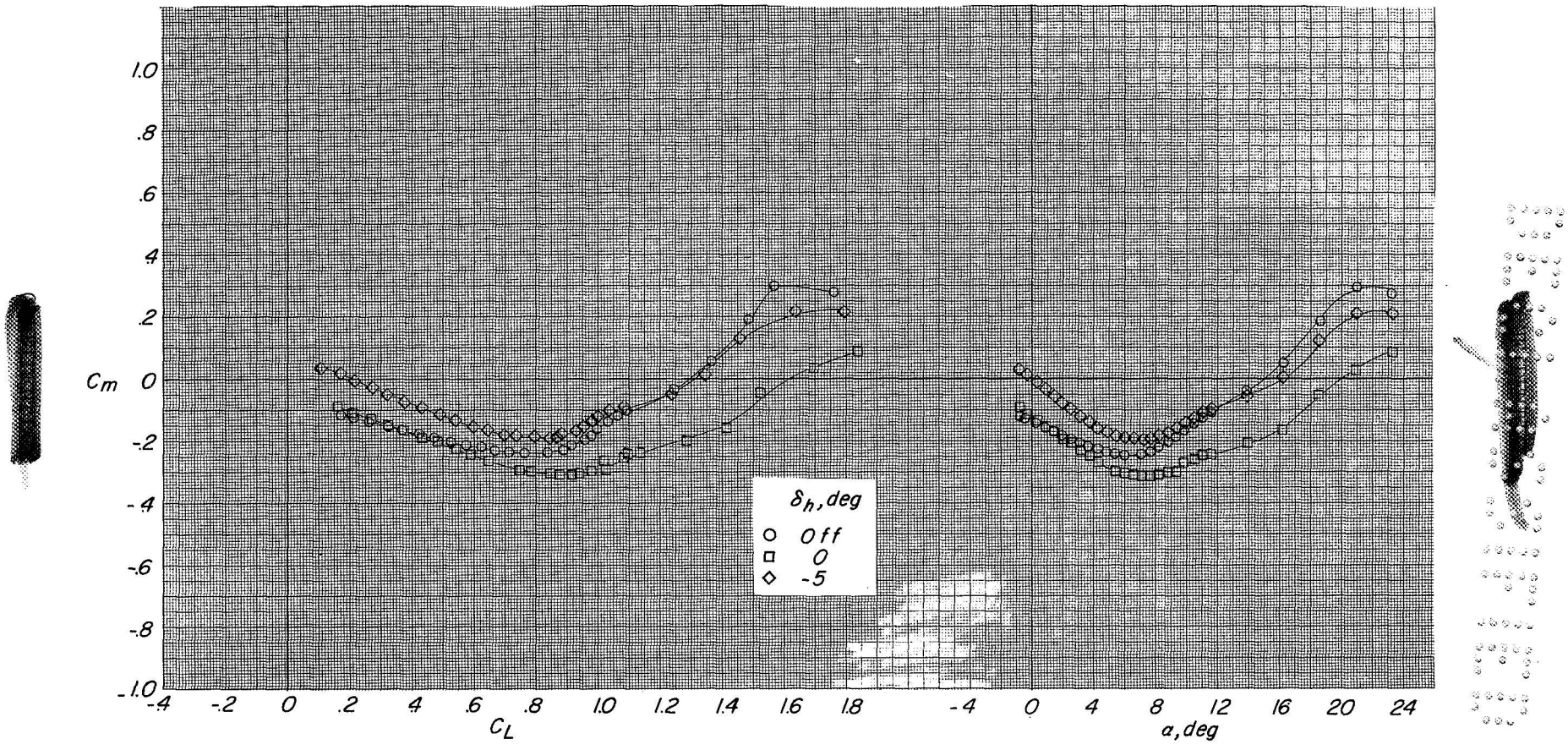

Figure 9.- Concluded.

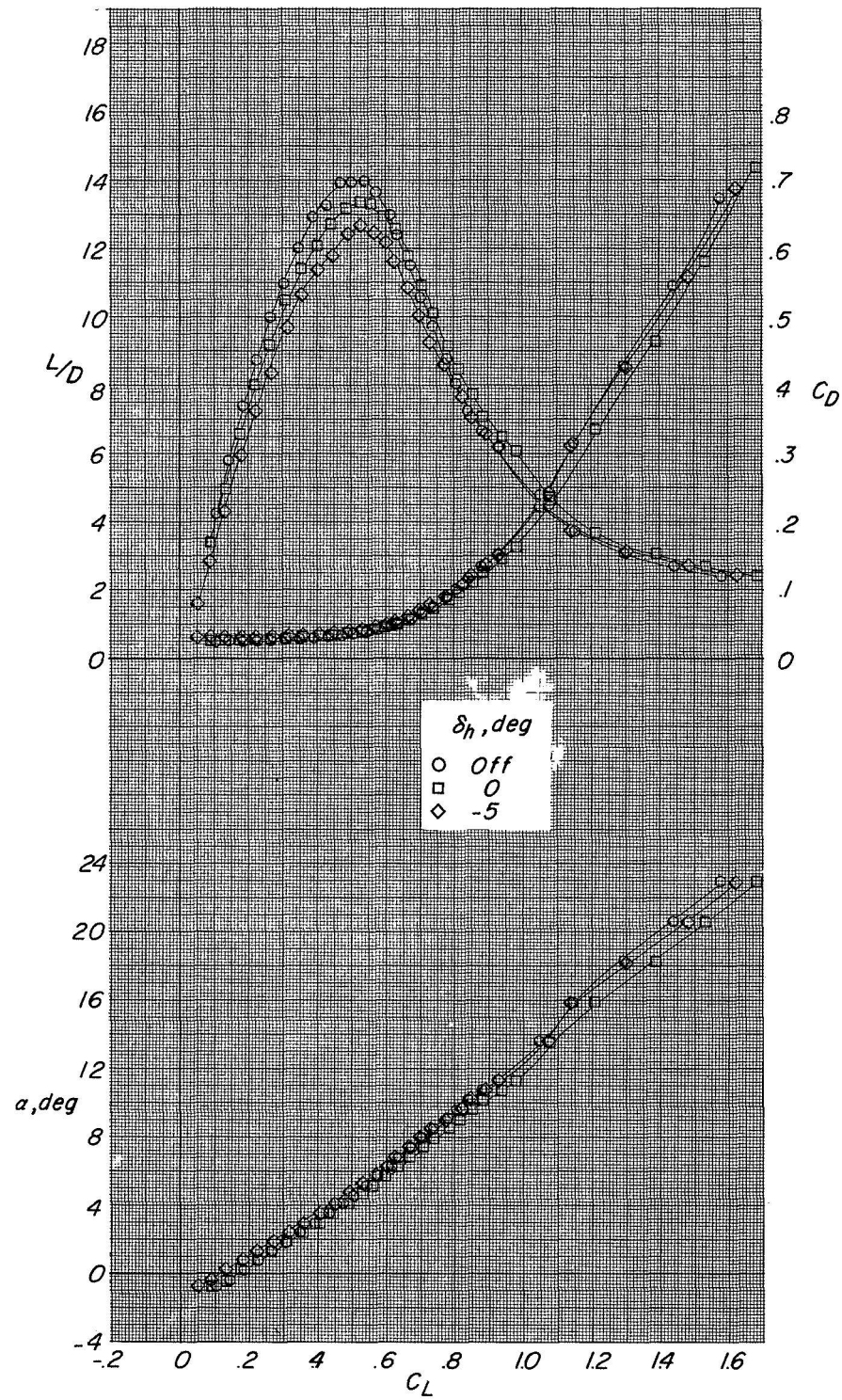

Figure 10.- Effect of horizontal tail on longitudinal aerodynamic characteristics. FWH_1V_N; $\Lambda = 46°$.

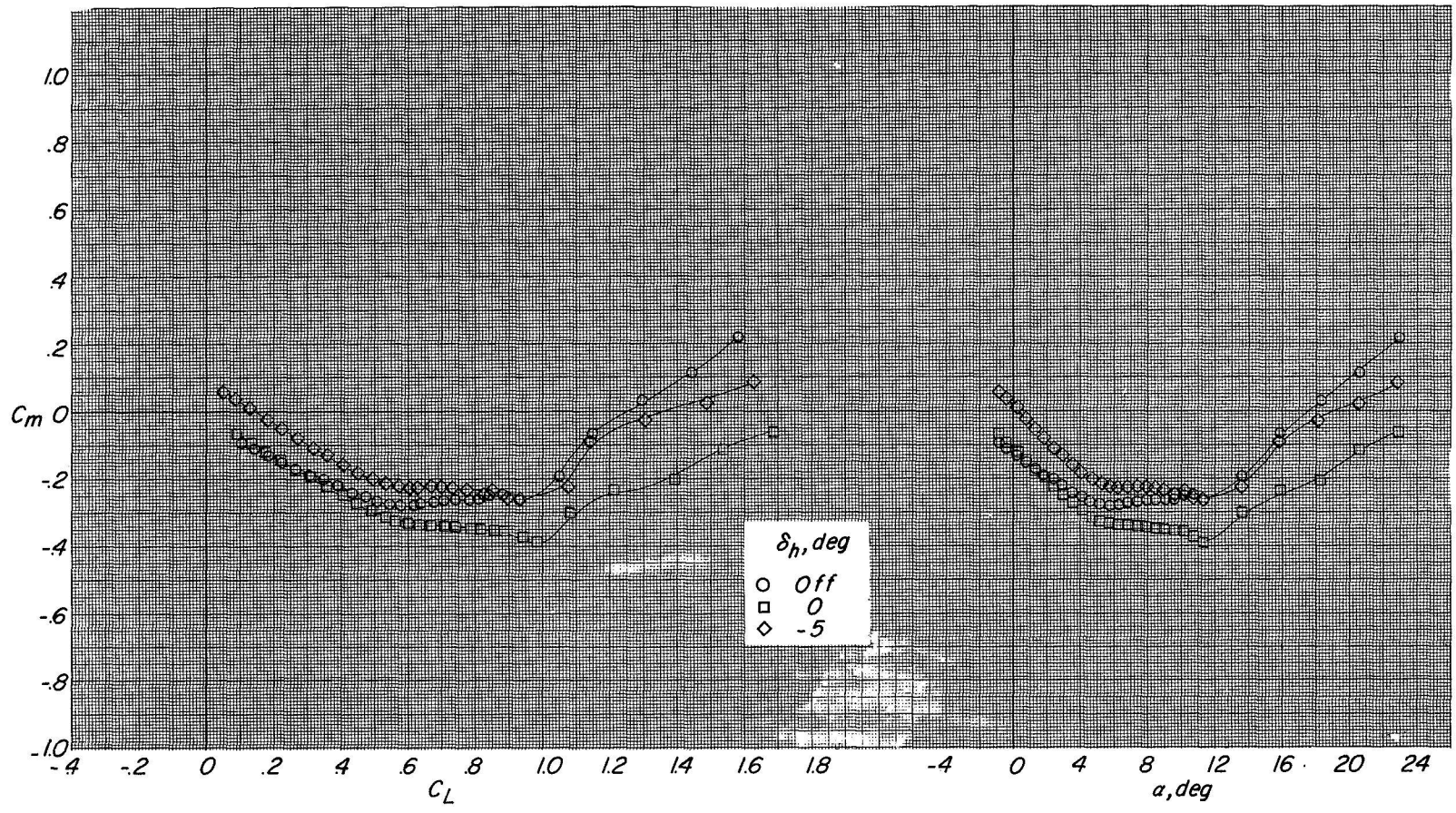

Figure 10.- Concluded.

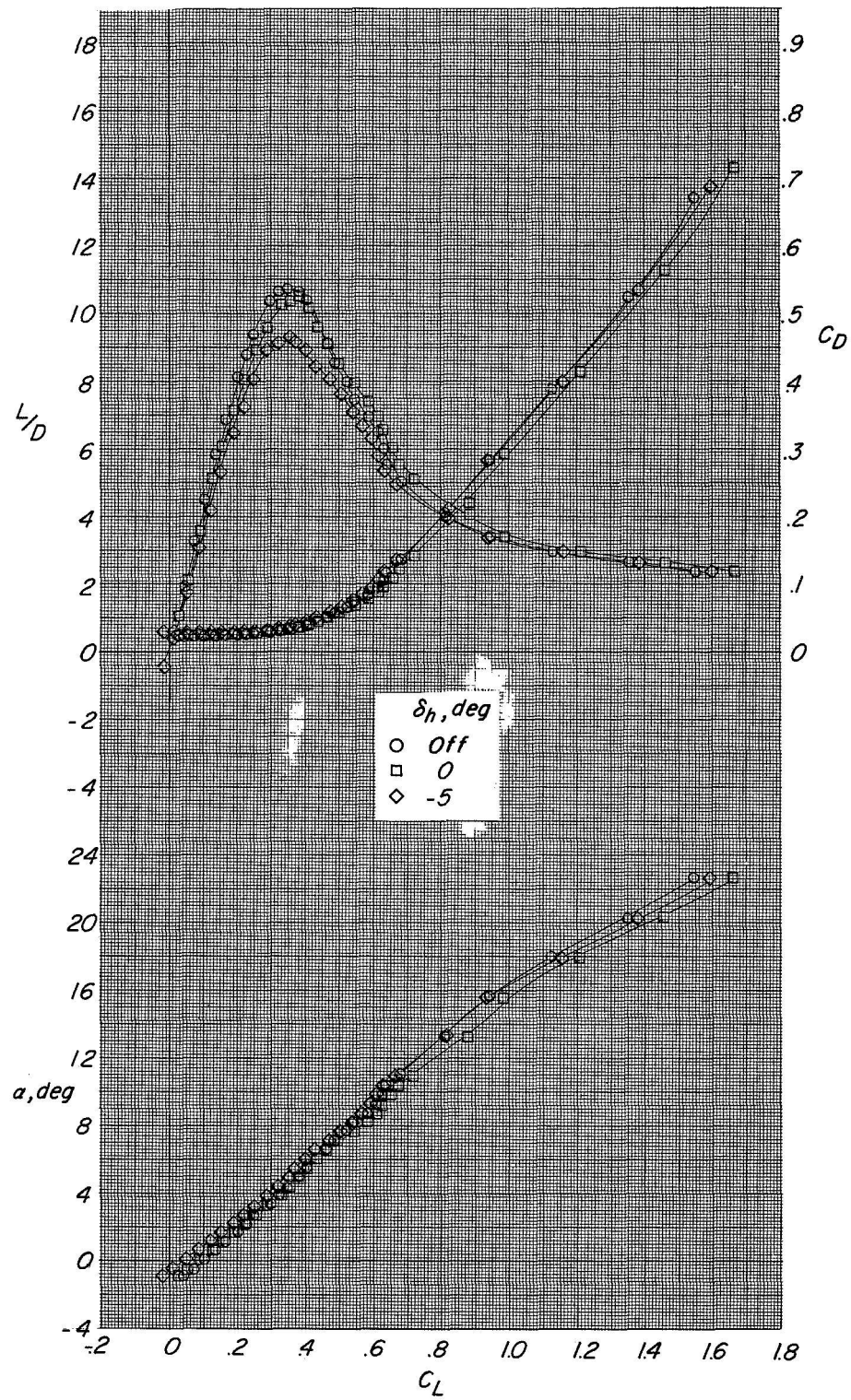

Figure 11.- Effect of horizontal tail on longitudinal aerodynamic characteristics. FWH_1V_TN; $\Lambda = 61^\circ$.

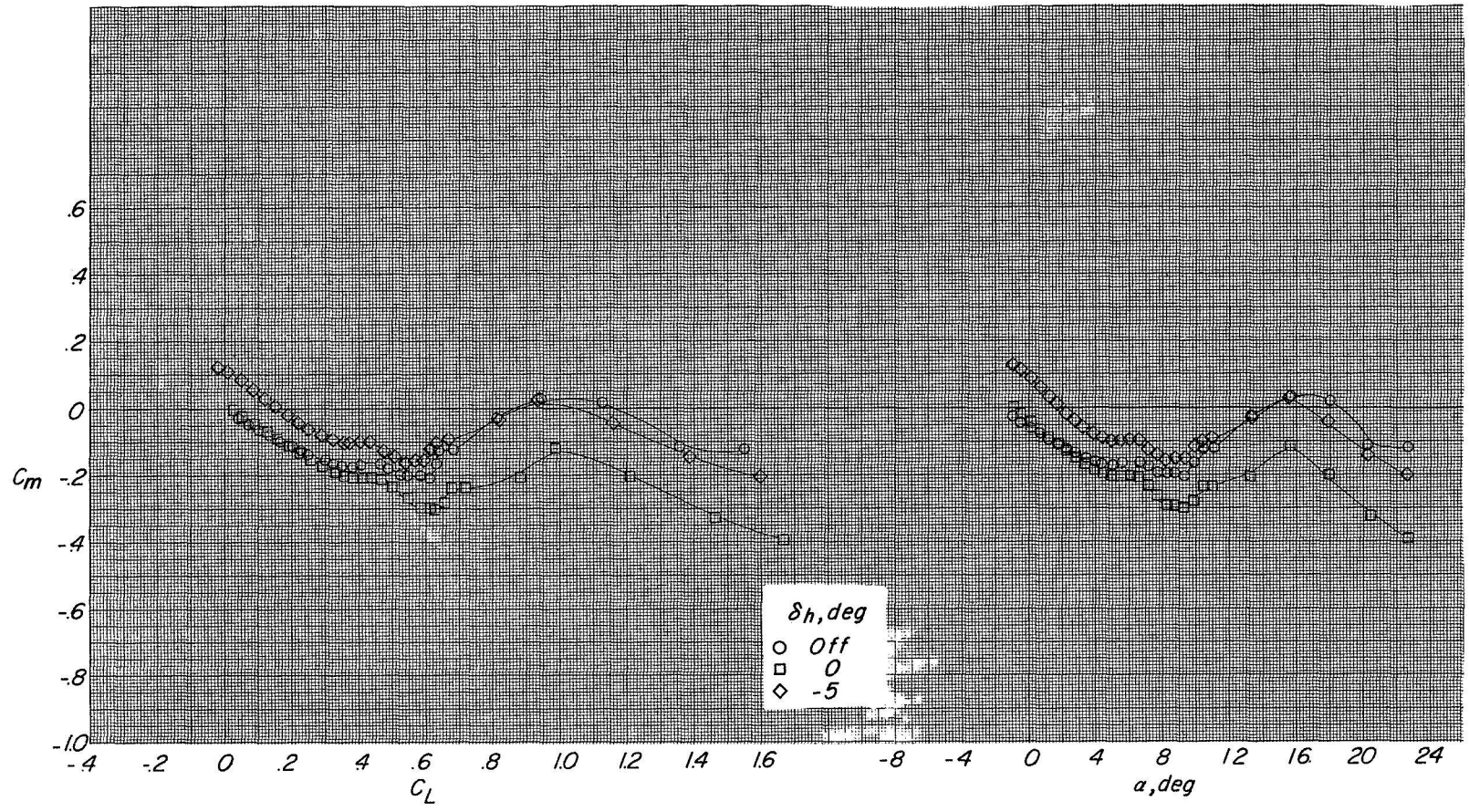

Figure 11.- Concluded.

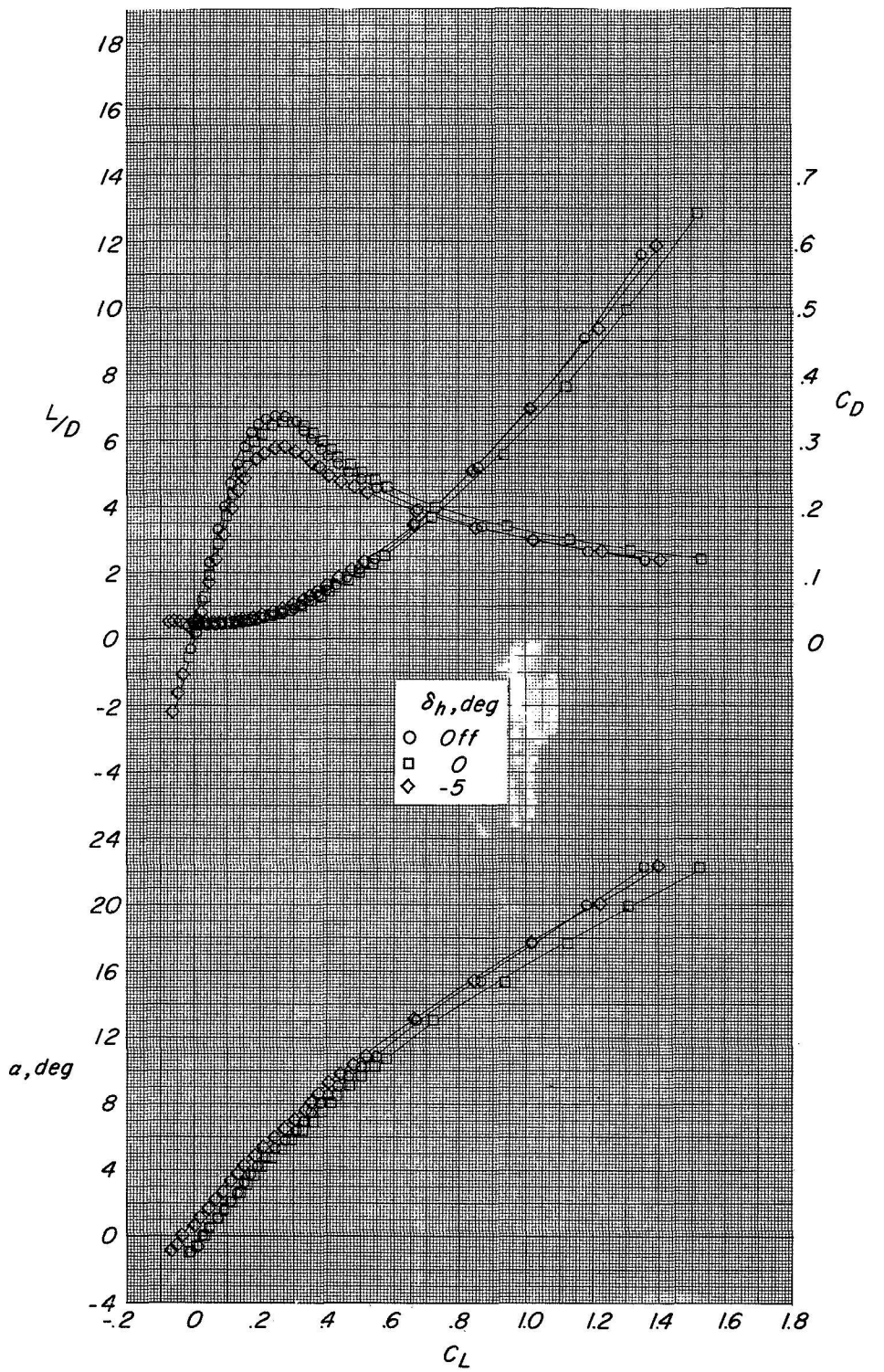

Figure 12.- Effect of horizontal tail on longitudinal aerodynamic characteristics. FWH_1V_NN; $\Lambda = 76^\circ$.

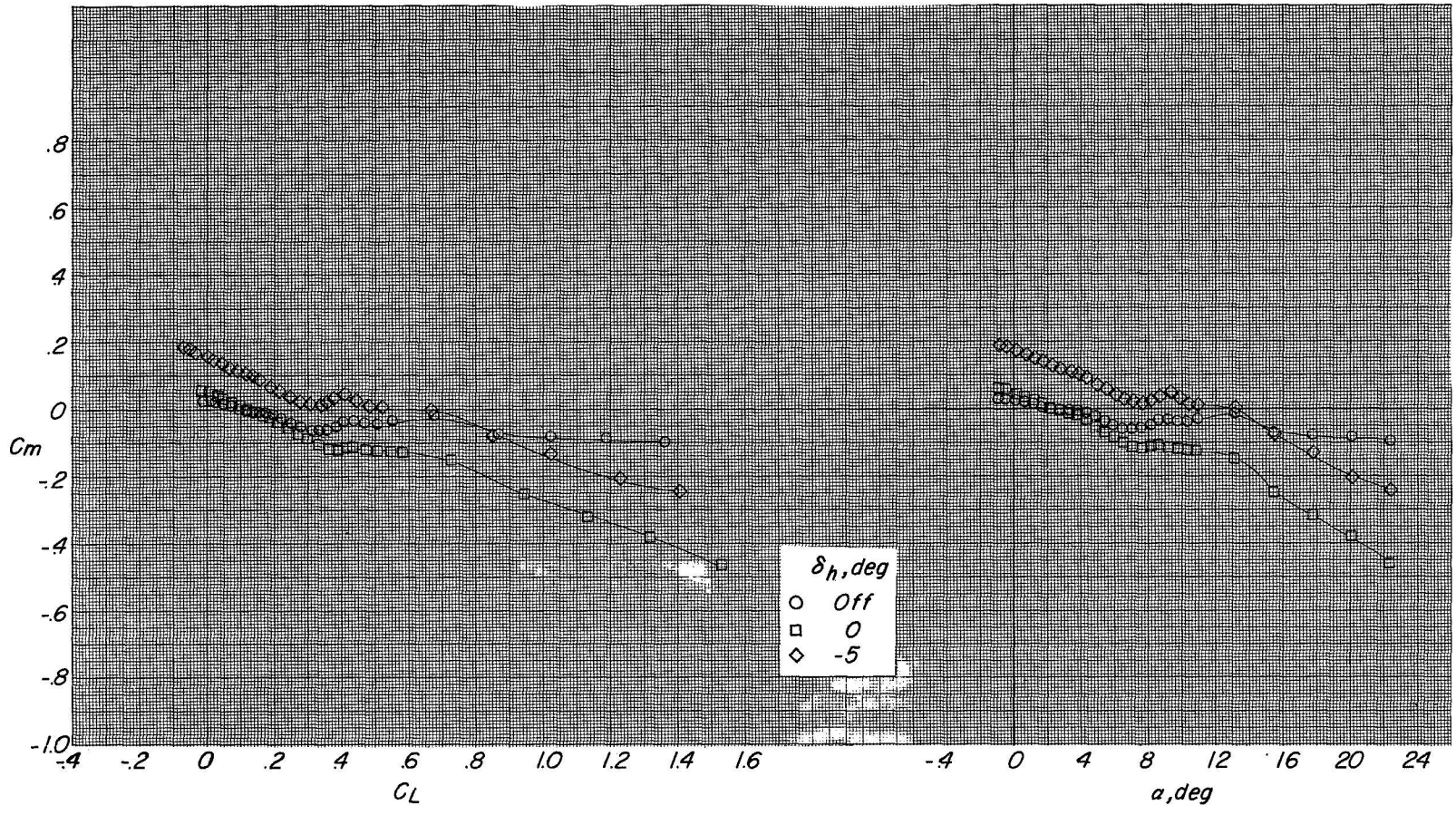

Figure 12.- Concluded.

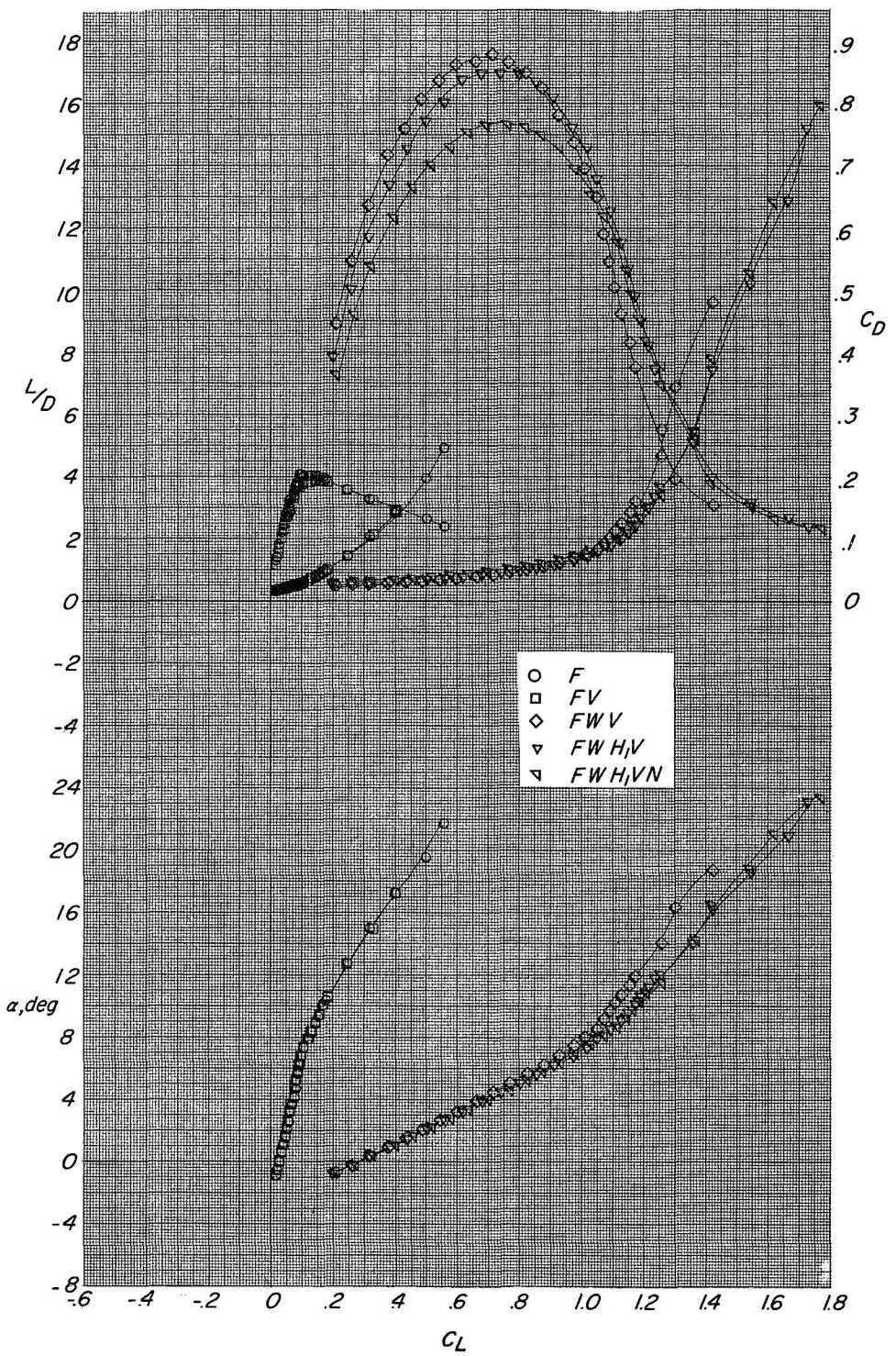

Figure 13.- Effect of model components on longitudinal aerodynamic characteristics. $\Lambda = 16^\circ$; $\delta_h = 0^\circ$.

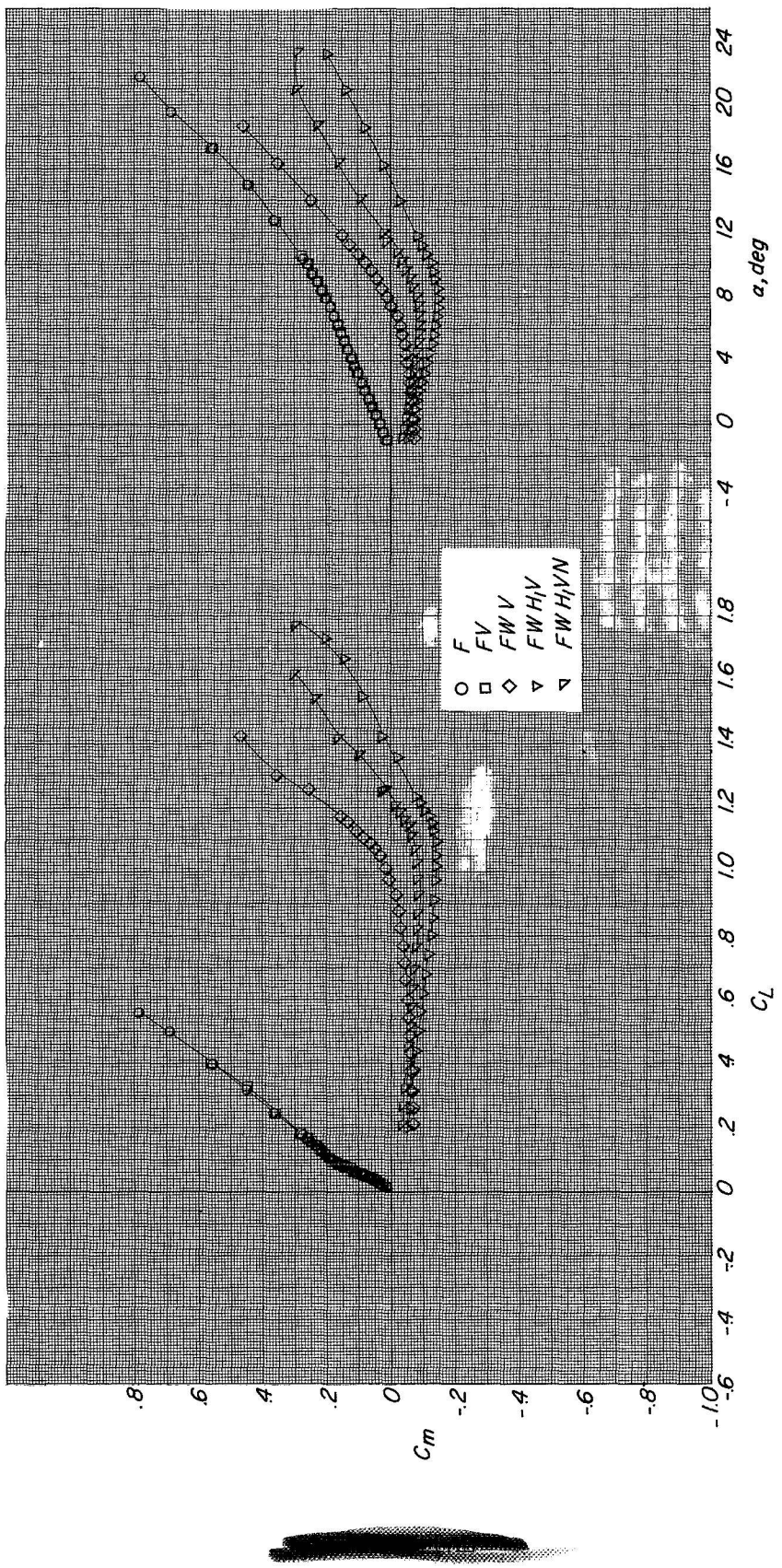

Figure 13.- Concluded.

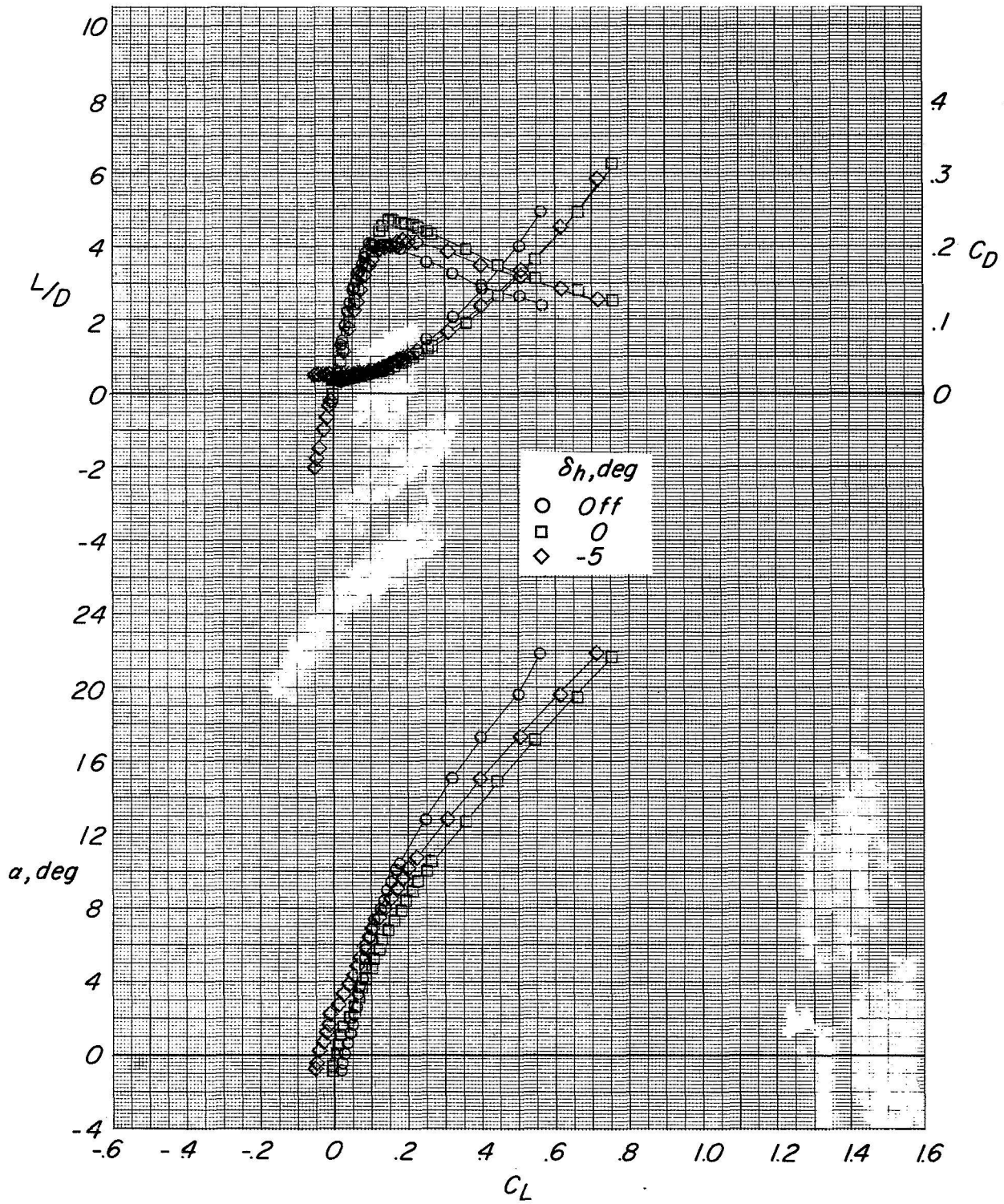

Figure 14.- Effect of horizontal tail on longitudinal aerodynamic characteristics. FH_1.

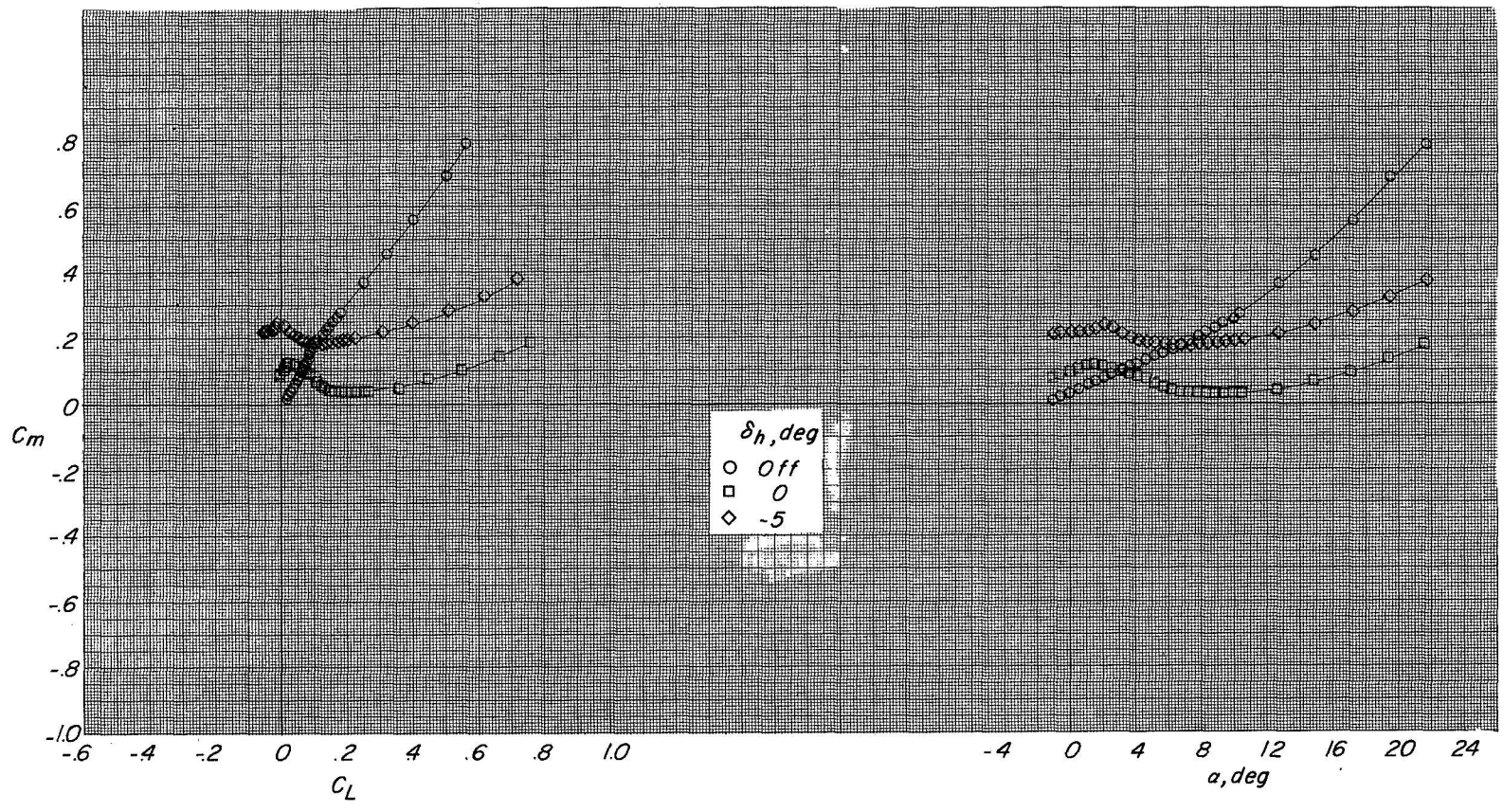

Figure 14.- Concluded.

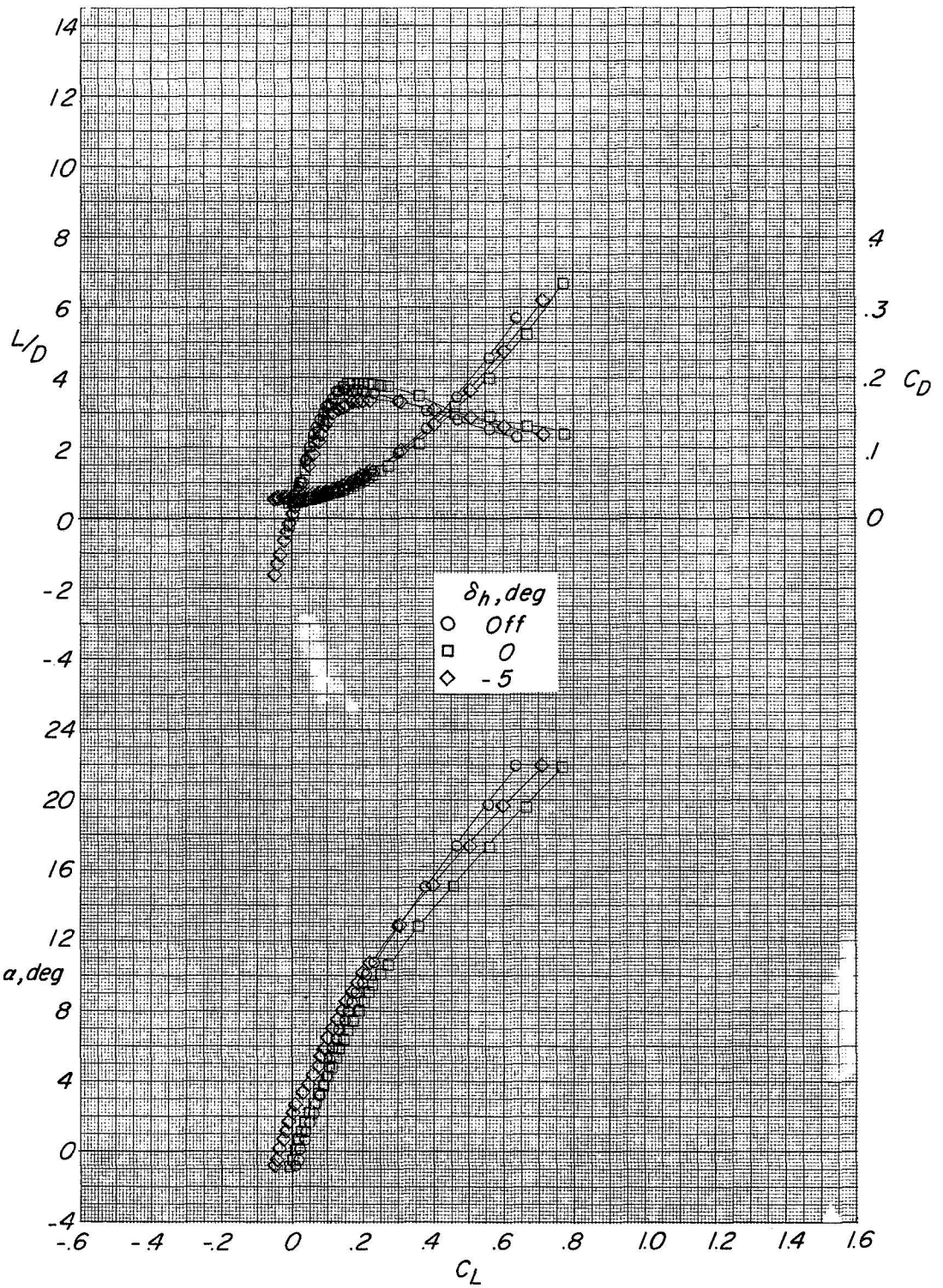

Figure 15.- Effect of horizontal tail on longitudinal aerodynamic characteristics. FH_1V_NN.

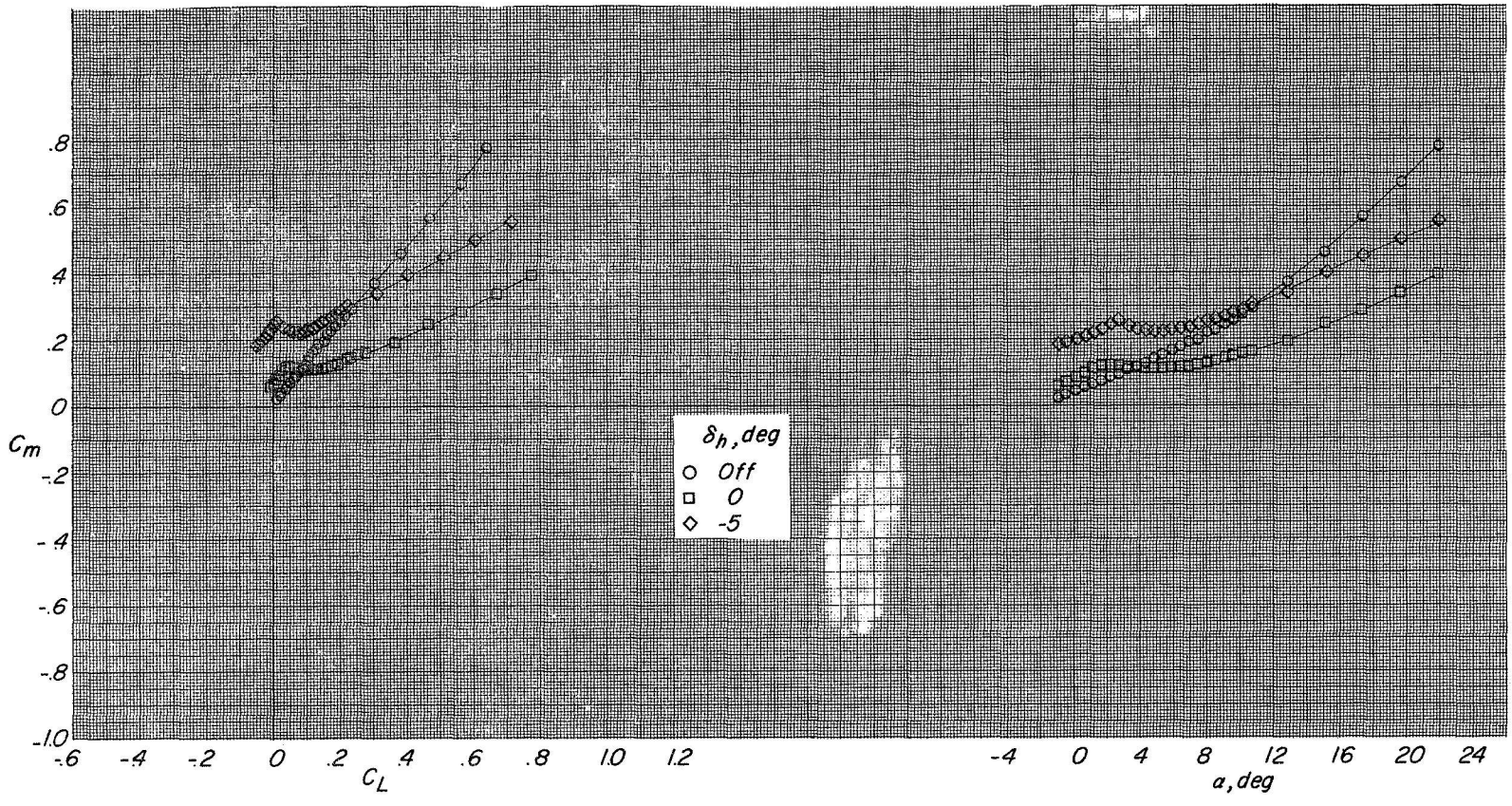

Figure 15.- Concluded.

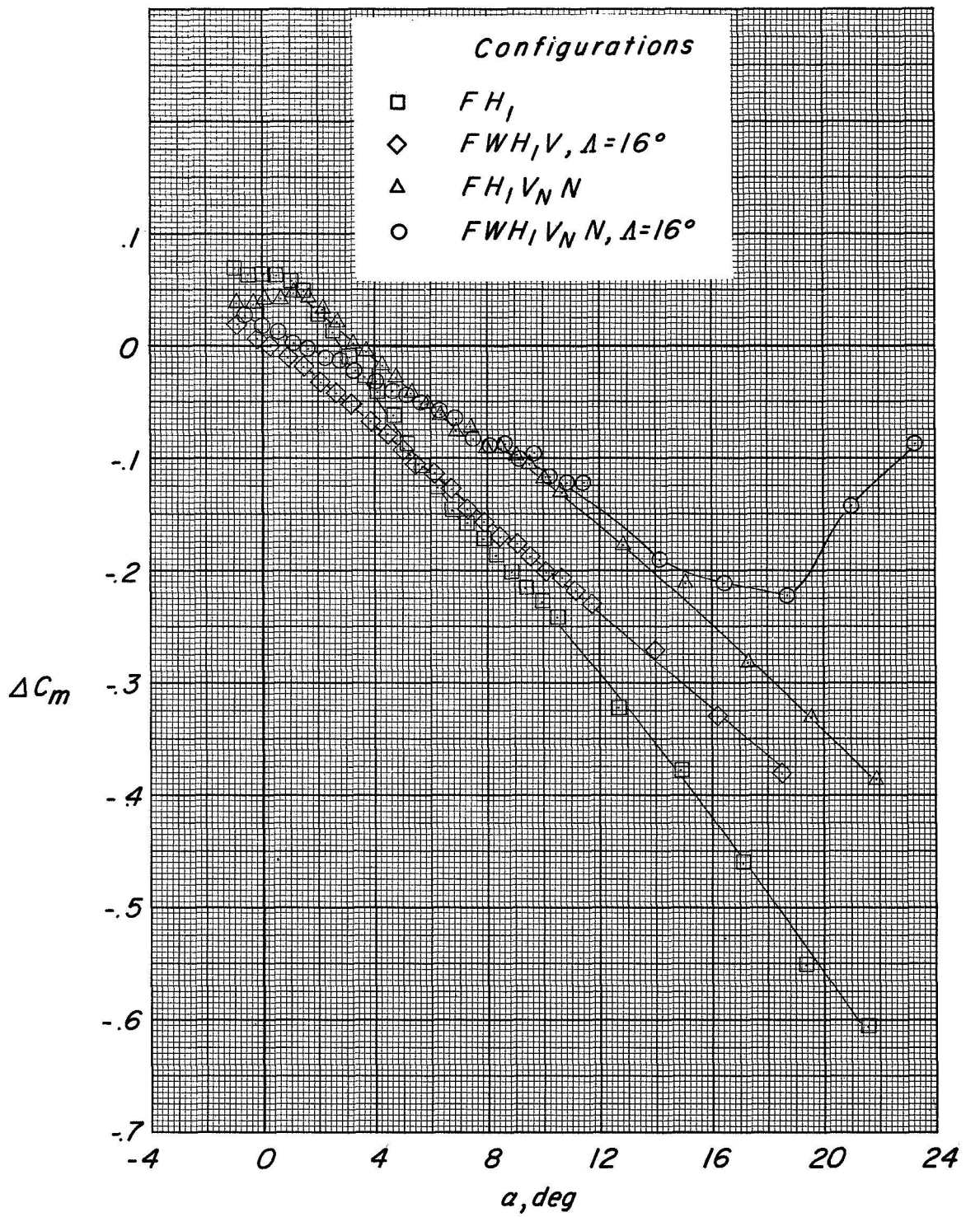

Figure 16.- Increment in pitching-moment coefficient due to addition of horizontal tail H_1 to various model configurations. $\delta_h = 0^\circ$.

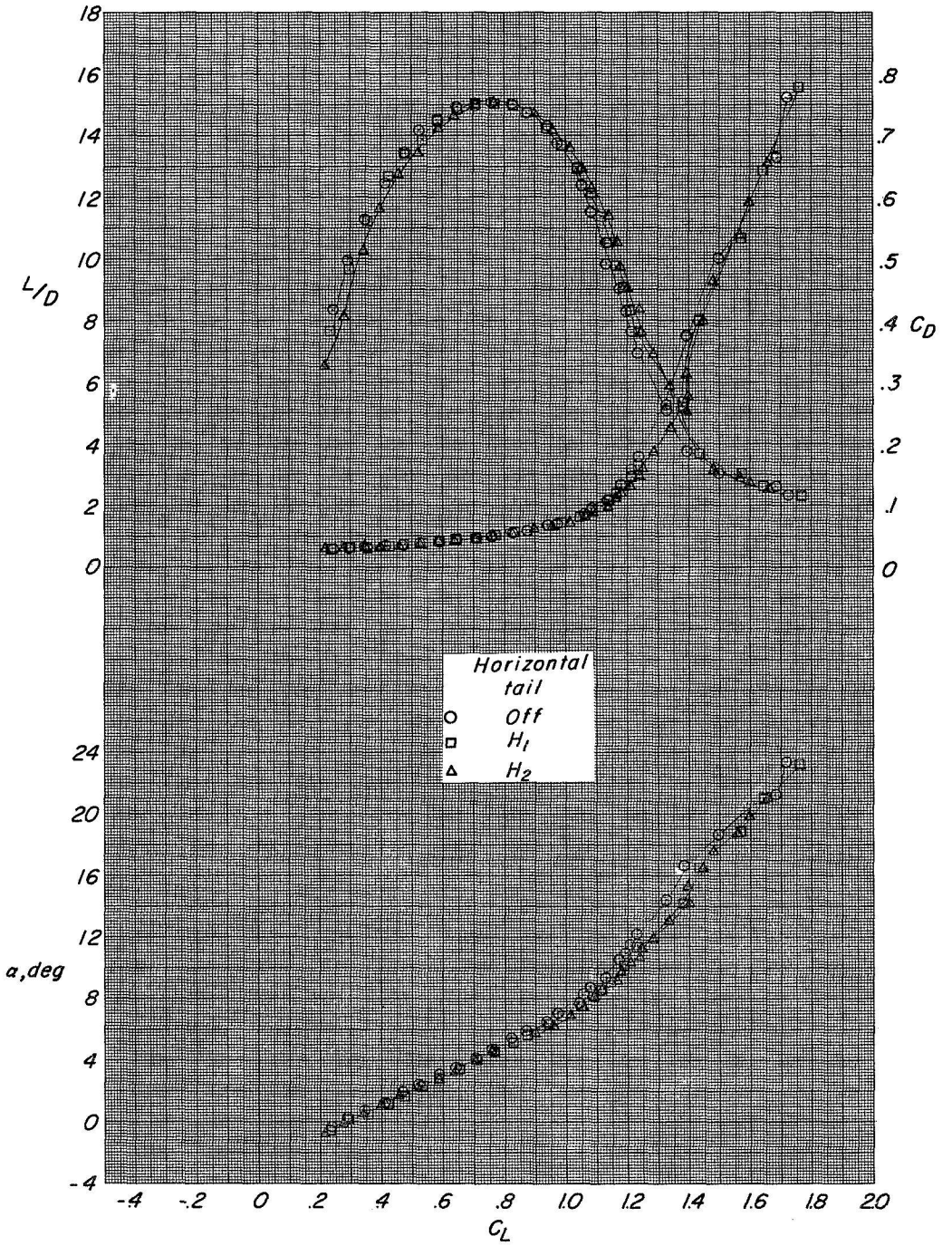

(a) H_1 and H_2.

Figure 17.- Effect of horizontal-tail configuration on longitudinal aerodynamic characteristics. $FWHV_NN$; $\Lambda = 16^\circ$; $\delta_h = 0^\circ$.

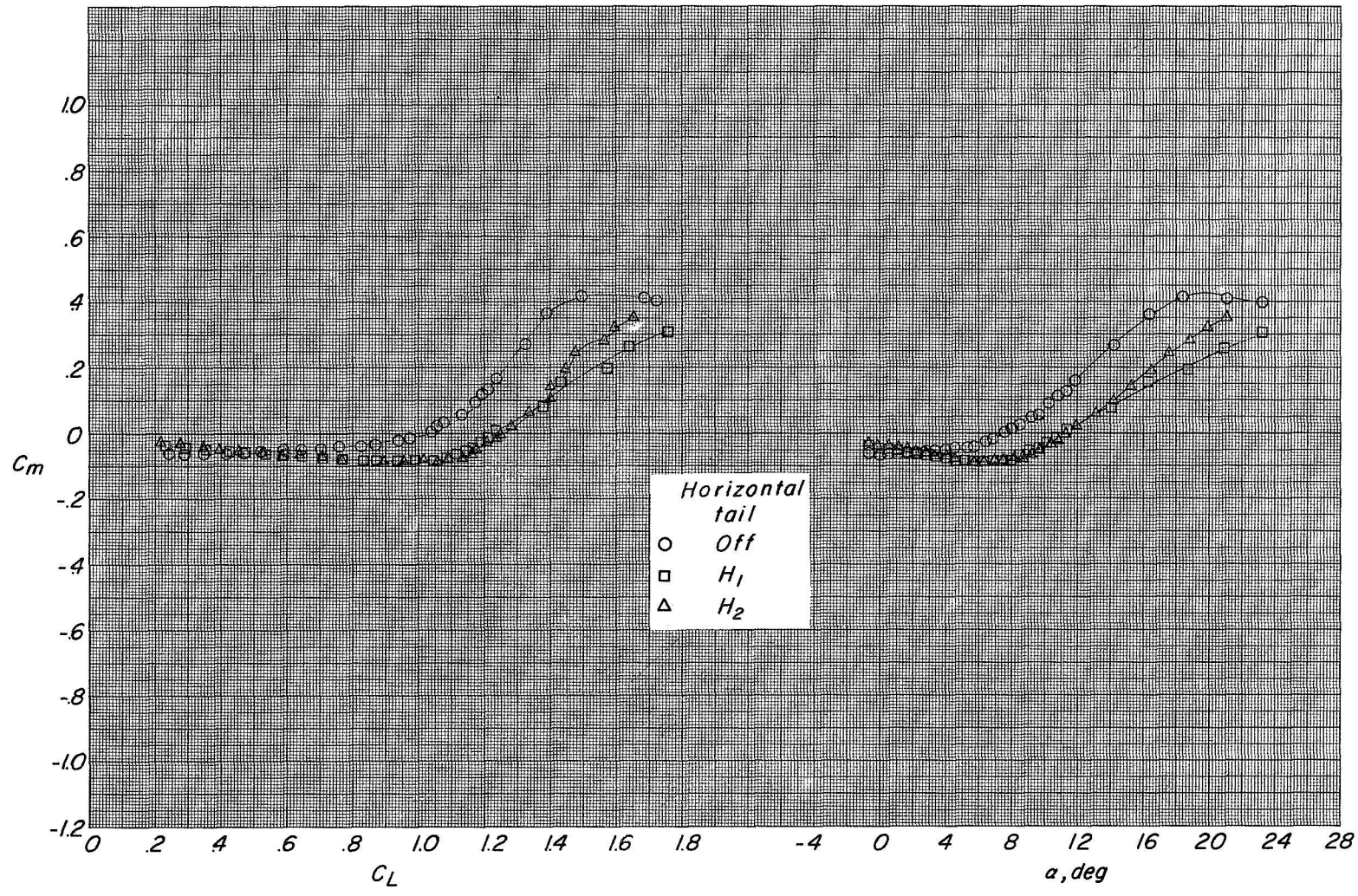

(a) Concluded.

Figure 17.- Continued.

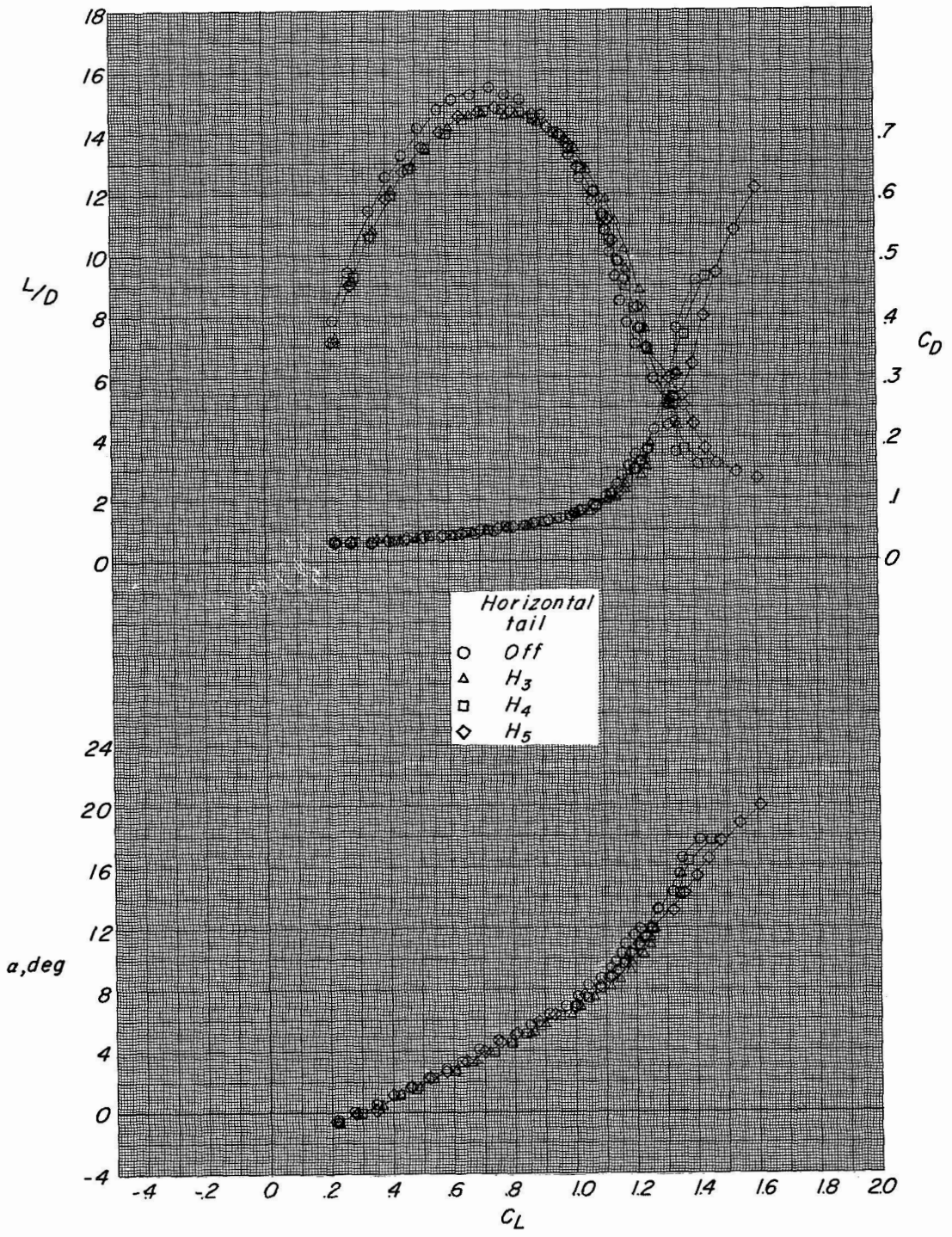

(b) H_3, H_4, and H_5.

Figure 17.- Continued.

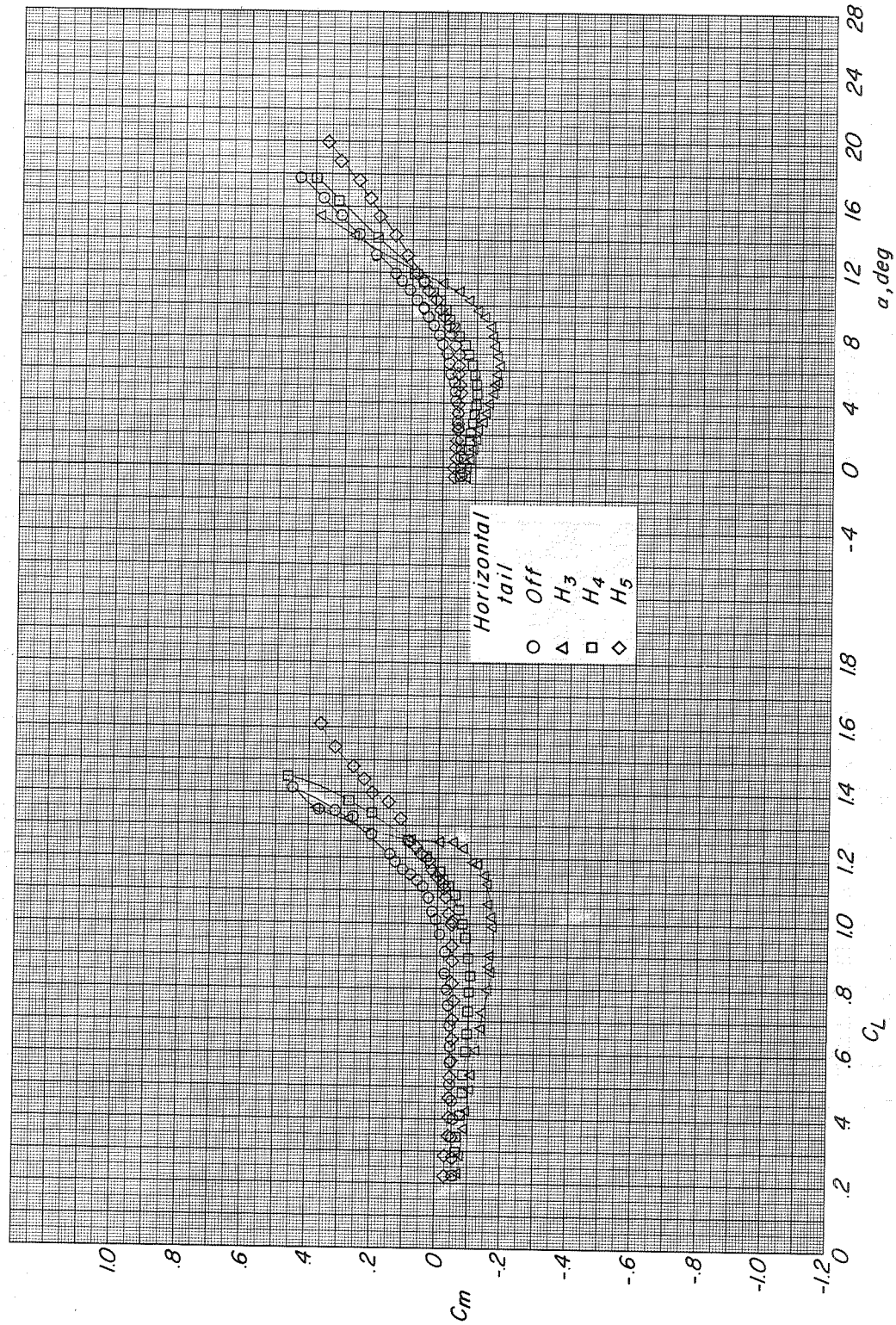

(b) Concluded.

Figure 17.- Concluded.

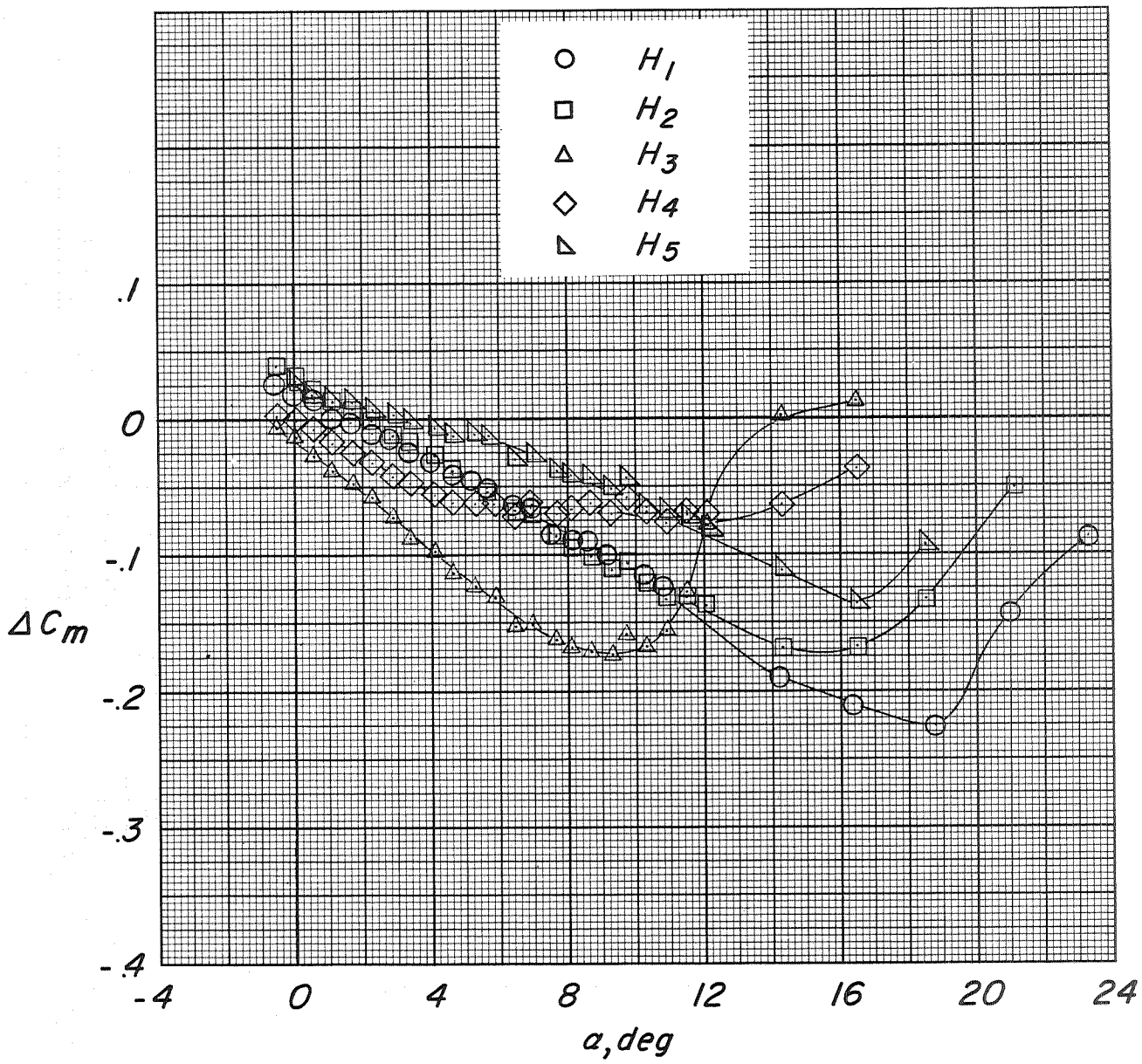

Figure 18.- Effect of horizontal-tail configuration on increment in pitching-moment coefficient due to addition of tail to model $FWHV_N N$. $\Lambda = 16^\circ$; $\delta_h = 0^\circ$.

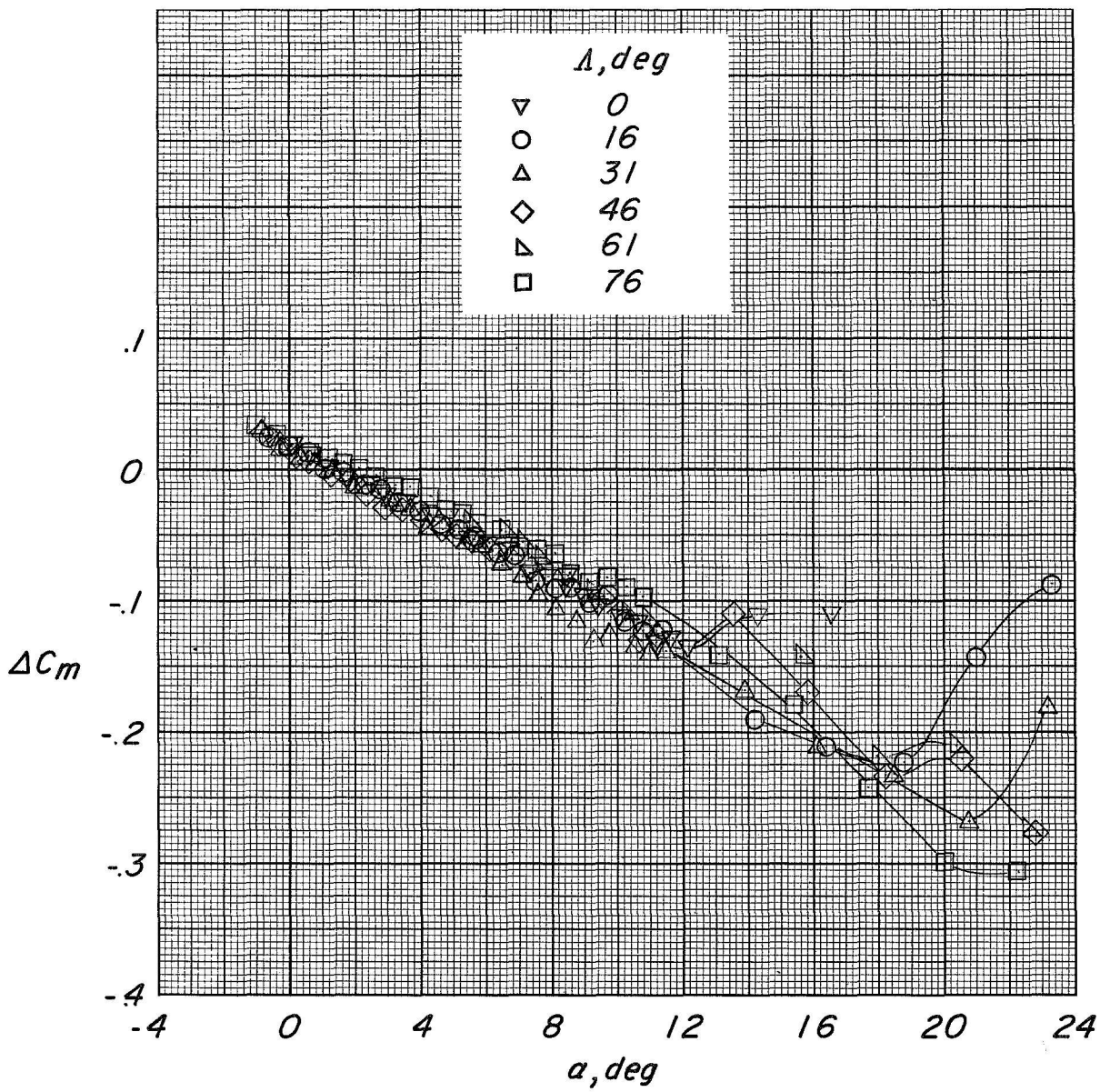

Figure 19.- Effect of wing sweep on increment in pitching-moment coefficient due to addition of horizontal tail. FWH_1V_NN; $\delta_h = 0^\circ$.

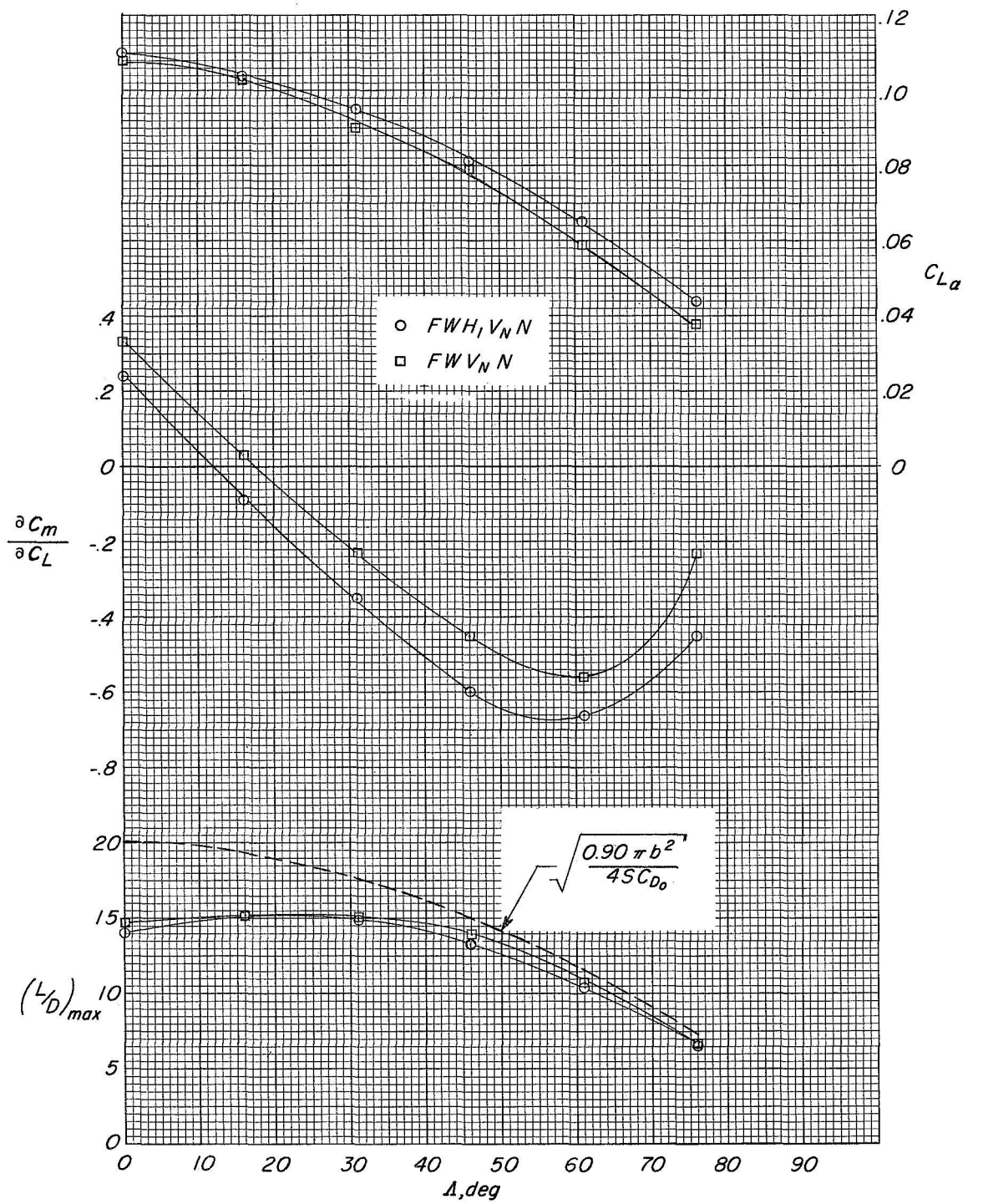

Figure 20.- Variation of C_{L_α}, $\partial C_m/\partial C_L$, and $(L/D)_{max}$ with wing sweep. FWV_NN and FWH_1V_NN.

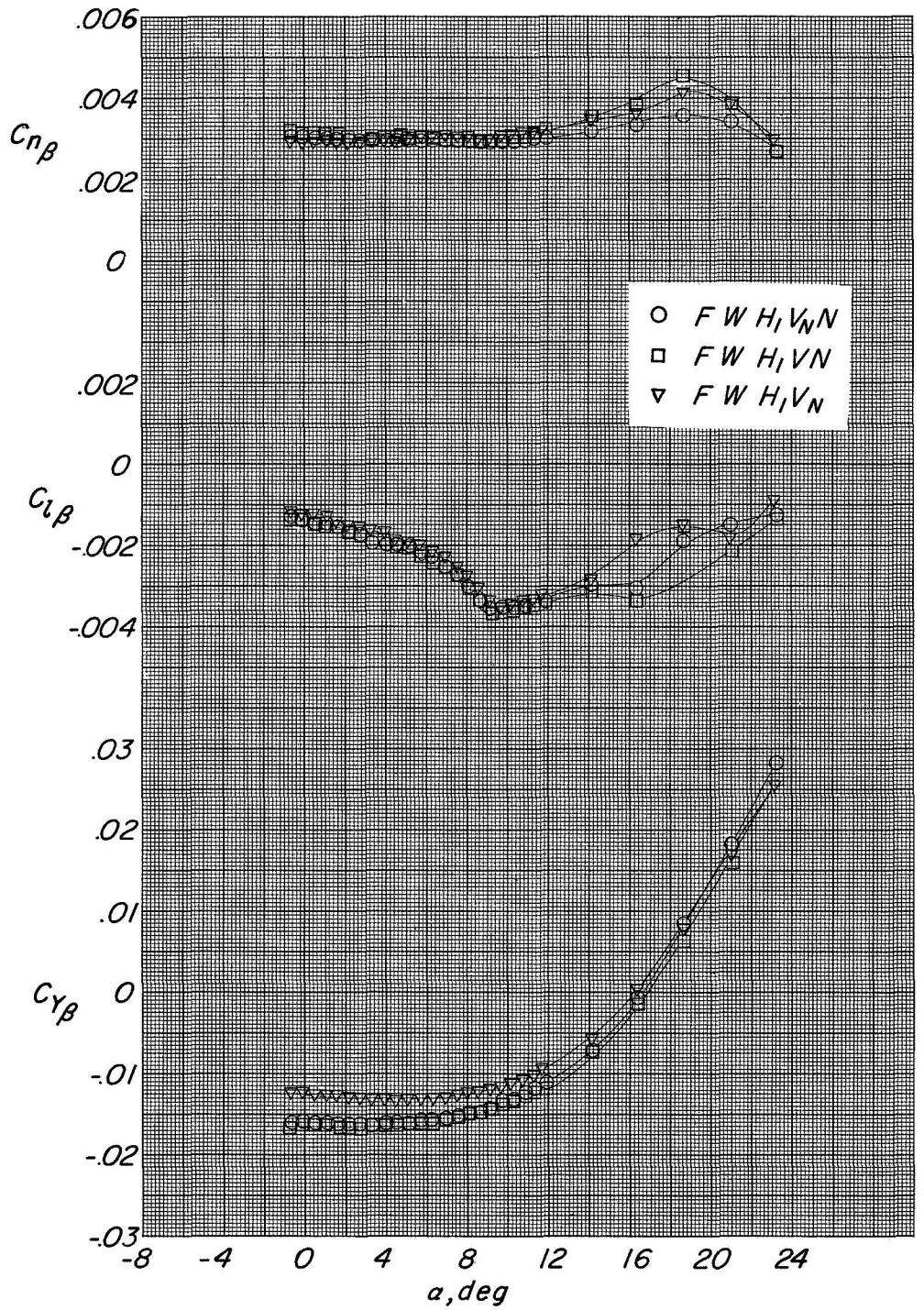

(a) $\Lambda = 16^{\circ}$.

Figure 21.- Effect of nacelles on lateral stability derivatives.

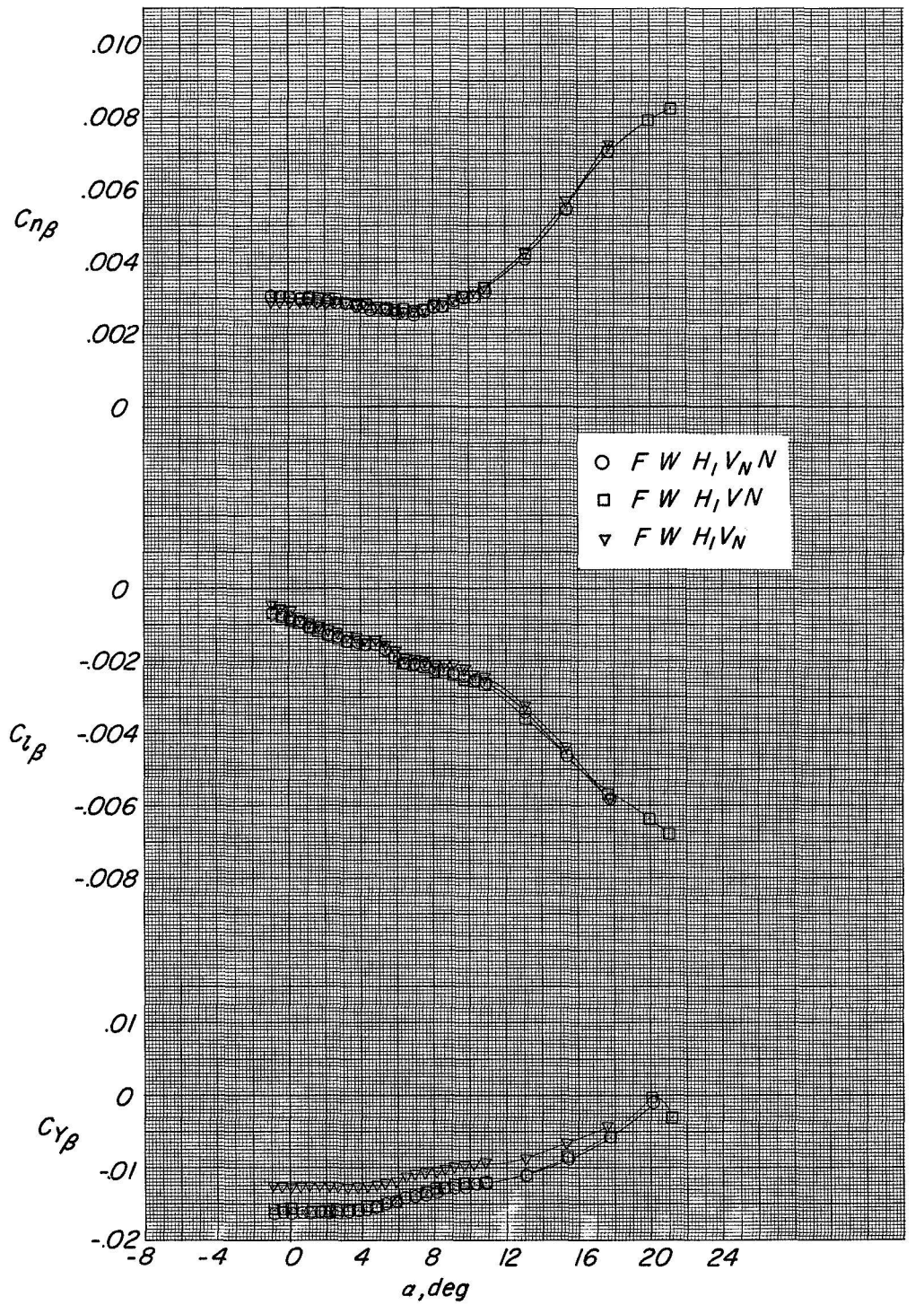

(b) $\Lambda = 76^{\circ}$.

Figure 21.- Concluded.

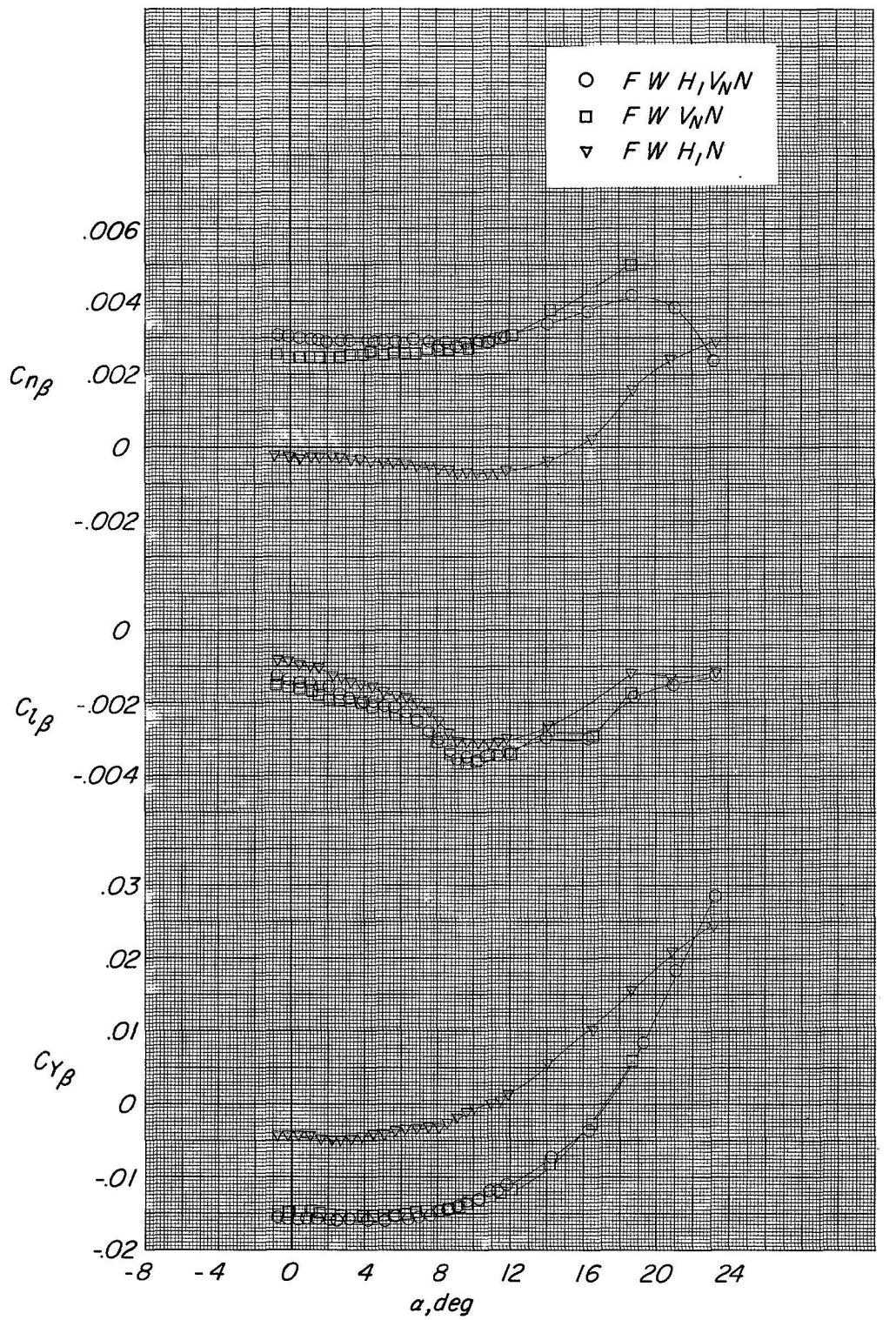

(a) $\Lambda = 16^\circ$.

Figure 22.- Effect of tail configuration on lateral stability derivatives.

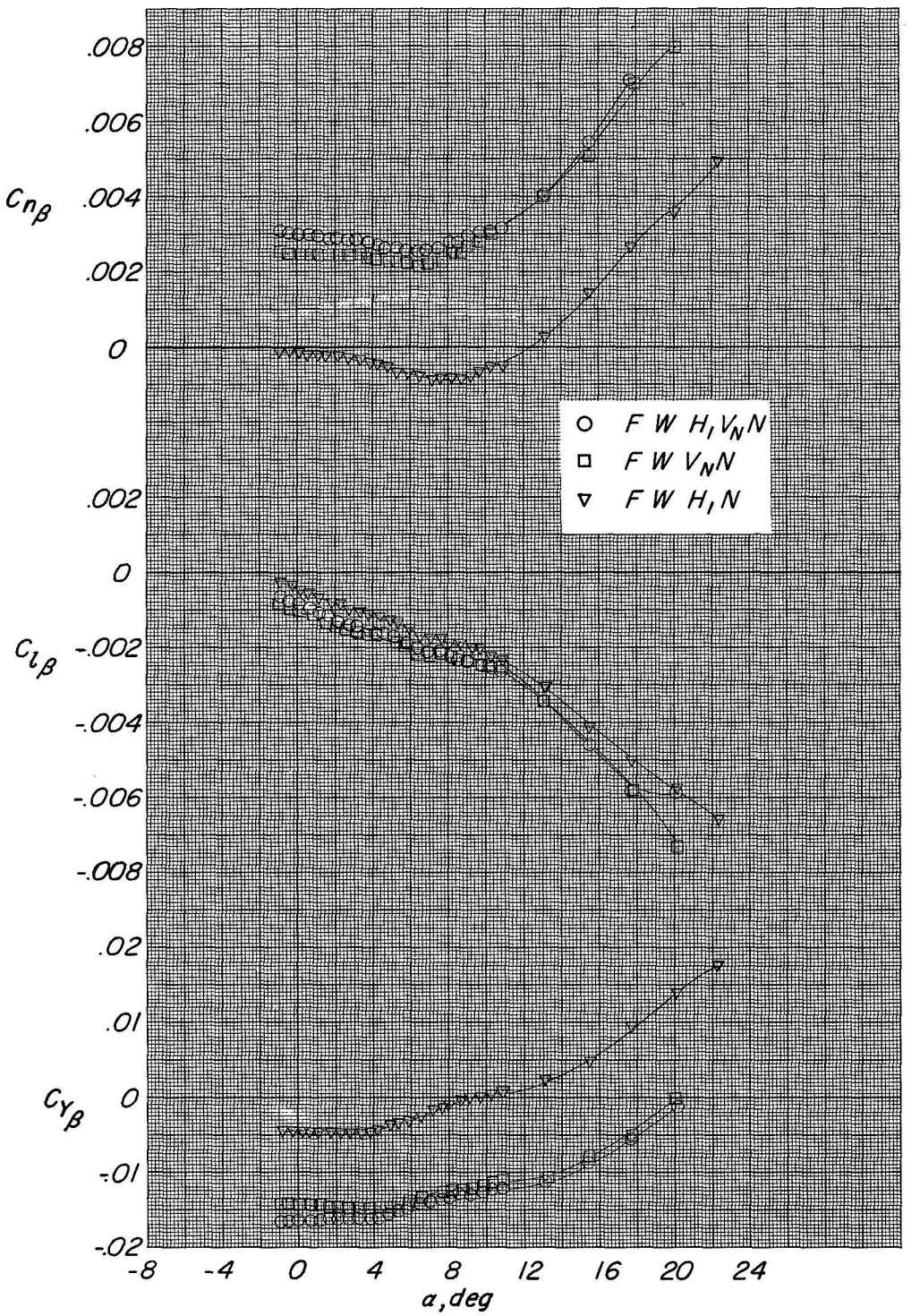

(b) $\Lambda = 76^\circ$.

Figure 22.- Concluded.

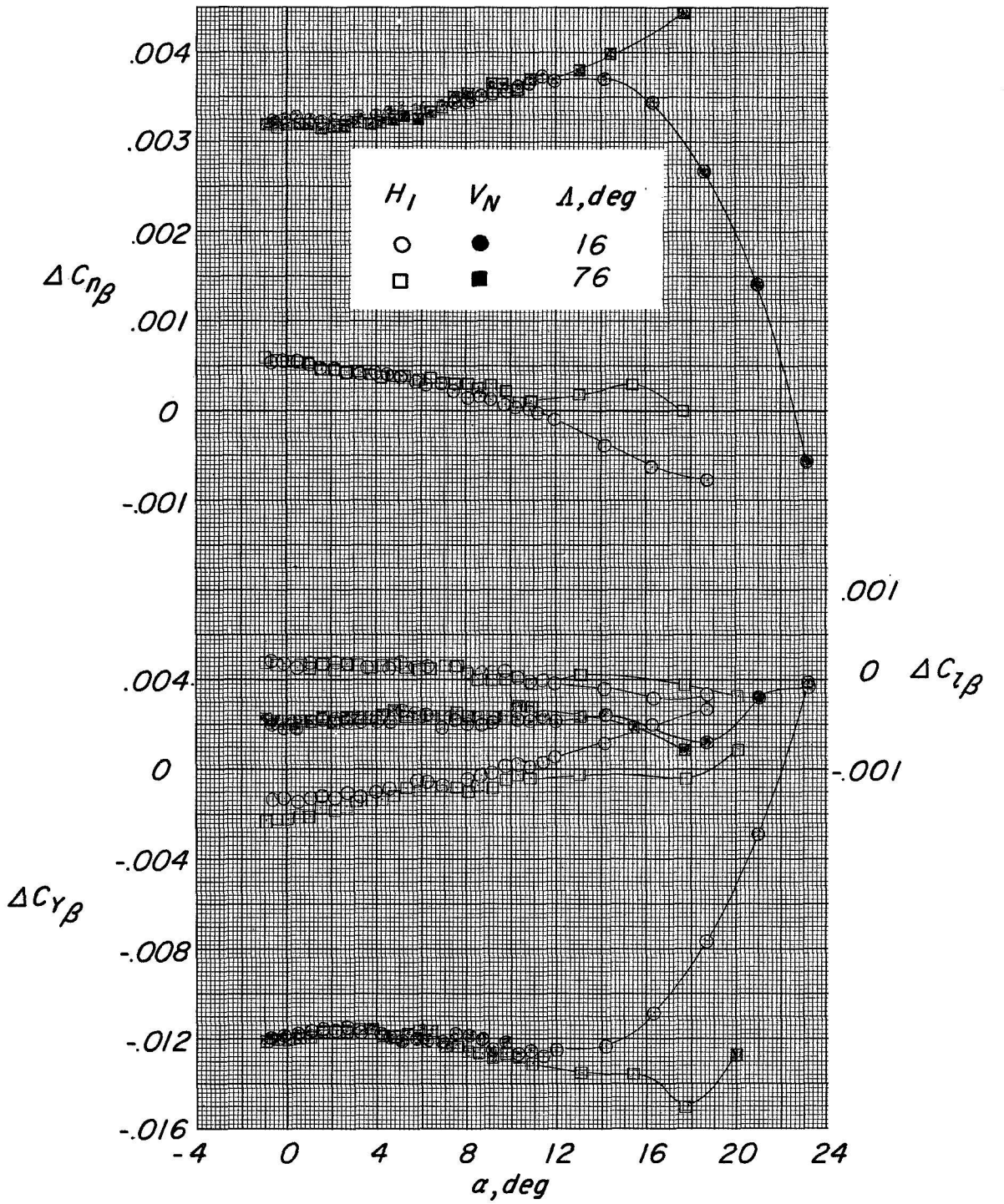

Figure 23.- Incremental effect of vertical tail and of horizontal tail on lateral stability derivatives. $\delta_h = 0^\circ$.

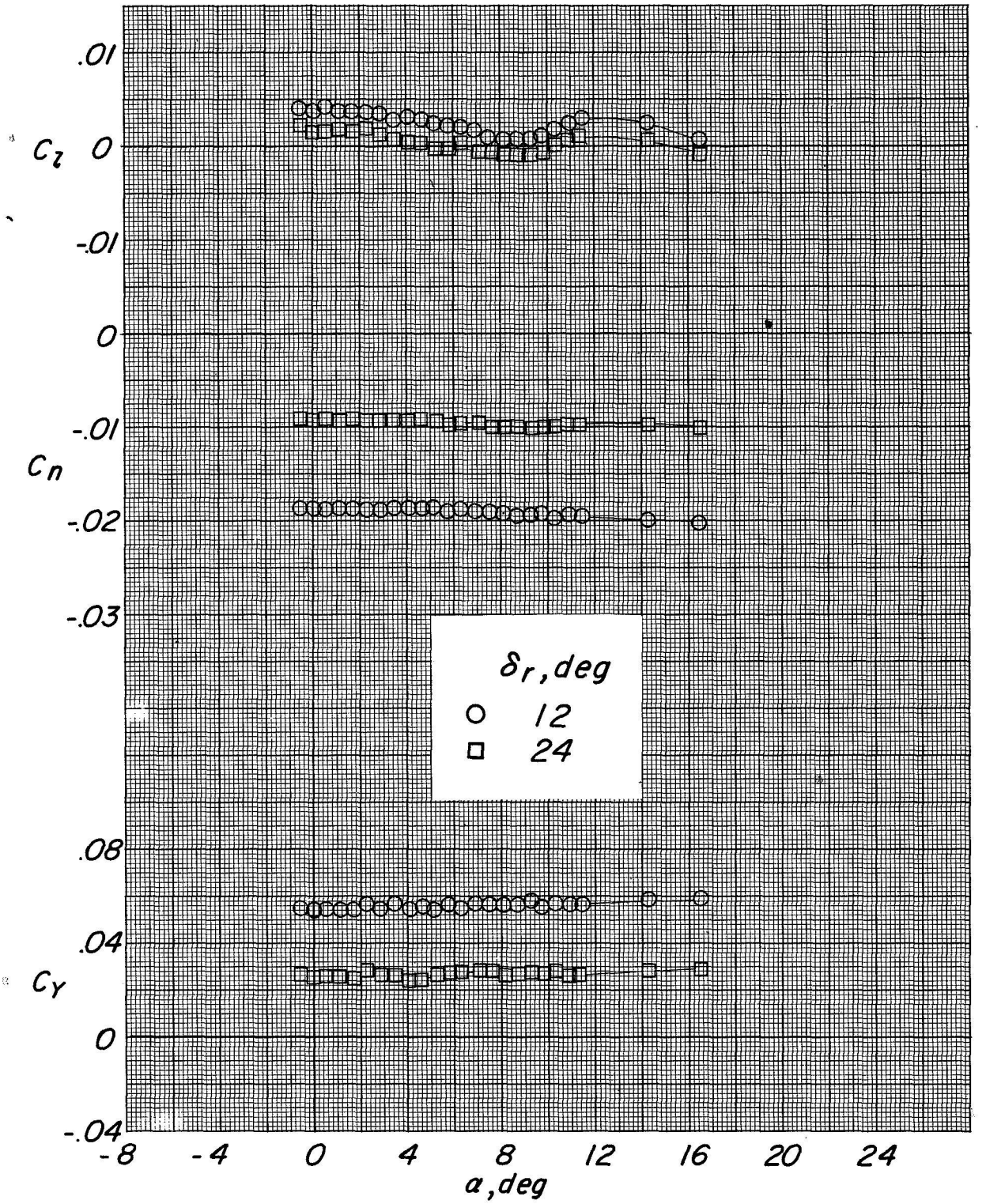

Figure 24.- Effects of rudder deflection on C_l, C_n, and C_Y. FWH_1V_NN; $\beta = 0^\circ$; $\delta_h = 0^\circ$; $\Lambda = 16^\circ$.

CONFIDENTIAL

"The aeronautical and space activities of the United States shall be conducted so as to contribute . . . to the expansion of human knowledge of phenomena in the atmosphere and space. The Administration shall provide for the widest practicable and appropriate dissemination of information concerning its activities and the results thereof."

—NATIONAL AERONAUTICS AND SPACE ACT OF 1958

NASA SCIENTIFIC AND TECHNICAL PUBLICATIONS

TECHNICAL REPORTS: Scientific and technical information considered important, complete, and a lasting contribution to existing knowledge.

TECHNICAL NOTES: Information less broad in scope but nevertheless of importance as a contribution to existing knowledge.

TECHNICAL MEMORANDUMS: Information receiving limited distribution because of preliminary data, security classification, or other reasons.

CONTRACTOR REPORTS: Technical information generated in connection with a NASA contract or grant and released under NASA auspices.

TECHNICAL TRANSLATIONS: Information published in a foreign language considered to merit NASA distribution in English.

TECHNICAL REPRINTS: Information derived from NASA activities and initially published in the form of journal articles.

SPECIAL PUBLICATIONS: Information derived from or of value to NASA activities but not necessarily reporting the results of individual NASA-programmed scientific efforts. Publications include conference proceedings, monographs, data compilations, handbooks, sourcebooks, and special bibliographies.

Details on the availability of these publications may be obtained from:

SCIENTIFIC AND TECHNICAL INFORMATION DIVISION

NATIONAL AERONAUTICS AND SPACE ADMINISTRATION

Washington, D.C. 20546

CONFIDENTIAL